Catalysis Science & Technology

Accepted Manuscript

This article can be cited before page numbers have been issued, to do this please use: M. Heshmat, L. Bruurs, C. De Kovel, F. van der Klis, R. K. Pazhavelikkakath Purushothaman, E. Hagberg and D. van Es, *Catal. Sci. Technol.*, 2026, DOI: 10.1039/D6CY00352D.




ROYAL SOCIETY OF CHEMISTRY

rsc.li/catalysis

View Article Online
DOI: 10.1039/D6CY00352D

# Mechanistic insights in the selective catalytic oxidation of glycolaldehyde: an industrially feasible route from biomass to bio-glycolic acid

Mojgan Heshmat*[a], Lotte Bruurs[a], Frits van der Klis*[a], Rajeesh Pazhavelikkakath Purushothaman[a], Erik Hagberg[b], Carolien de Kovel[c], Daan S. van Es*[a]

[a]Wageningen Food & Biobased Research, Bornse Weilanden 9, 6708 WG Wageningen, The Netherlands

[b]Archer Daniels Midland Company, 1001 N Brush College Road, Decatur, IL, 62521, USA

[c]Biometris, Wageningen University & Research, POBox 16, 6700 AA Wageningen, The Netherlands



## Abstract:

Glycolic acid (GAc) is used in a variety of applications, e.g., in the textile and leather industry, in dermatology and cosmetics and as a monomer to produce biodegradable polyglycolic acid (PGA) for e.g. biodegradable packaging. Currently, GAc is mainly produced from fossil feedstocks. To improve sustainability and circularity, a bio-based route is highly desirable. Pyrolysis of glucose and other monomeric sugars is an effective way to produce glycolaldehyde (GAl) from agricultural side streams. Hence, the selective catalytic oxidation of GAl to GAc is of scientific as well as industrial interest. Due to high reactivity of GAl, it is challenging to reach high selectivities (required for many applications) at industrially relevant conversions. Here we report the catalytic oxidation of GAl to glycolic acid using a Pt/C catalyst. Our experimental results show high selectivity at high conversion, while maintaining a high carbon balance under DoE optimised reaction conditions. The impact of oxygen pressure, catalyst:substrate ratio, and substrate concentration, as well as pH effects and product inhibition are addressed. Catalyst stability tests and characterisations (HAADF-STEM, BET, XRD, XPS, Elemental analysis) confirm that Pt/C is a promising catalyst for the selective oxidation of GAl to GAc. The experimental results are rationalized by employing DFT-metadynamics simulations at the finite reaction temperature and heterogeneous phase, where the entire reaction mechanism and network of main and side products are investigated and the key-elementary steps identified.

View Article Online
DOI: 10.1039/D6CY00352D





## Introduction

The development of a circular biobased economy is a prerequisite for countering the increasing detrimental effects of climate change caused by greenhouse gas emissions. However, care must be taken to use sustainable biomass feedstocks as well as green catalytic chemical conversion methods. Carbohydrate rich residues from agro-food processing and non-food biomass production (e.g. timber, pulp and paper) are an interesting feedstock stream for the production of added value circular chemicals and materials. To this end, different conversion technologies are currently being developed and implemented, including e.g. fermentation, electrochemical and chemocatalytic methods. Another interesting method is the pyrolysis crop residues like wood residues, corn stover or grey starches. Depending on the conditions used this can lead to e.g. the C6 platform chemical levoglucosenone or the C2 building block glycolaldehyde. Recently it was reported that the pyrolysis of glucose and other monomeric sugars under specific conditions can lead to high yields (>70%) of glycolaldehyde.[1-4] Glycolaldehyde is the shortest aldose with both an aldehyde and hydroxy groups, a highly reactive molecule found in the biosphere and interstellar space. Glycolaldehyde can be produced in various processes, such as the oxidation of isoprene or the decomposition of carbohydrates.[5,6] Since glycolaldehyde is very reactive and has limited direct applications there is great interest in further conversion into more stable, existing industrial chemicals, such as ethylene glycol[7,8] or glycolic acid[9,10].

Glycolic acid (2-hydroxyethanoic acid, $C_2H_4O_6$) is the smallest bifunctional α-hydroxy acid. It is used in a variety of applications, for example in the textile and leather industry, in dermatology and cosmetics or as a monomer to produce polyglycolic acid (PGA) and poly(lactic-co-glycolic acid) (PLGA). Polyglycolic acid can be used for production of biodegradable packaging applications. Glycolic acid is currently produced from petrochemical sources, mainly by carbonylation of formaldehyde to glycolic acid by using syngas, and by hydrolysis of monochloroacetic acid. It is desirable if glycolic acid can be produced from biomass, to make PGA not only bio-degradable, but also bio-based. Several studies have reported heterogeneous/homogeneous catalysts for glycolaldehyde oxidation. Homogenous molybdenum based heteropolyacids are reported for conversion of cellulosic biomass to GA, however, toxicity of this catalyst is a main drawback.[11] Overall, toxicity, rigorous reaction conditions and low selectivity of oxidation triggered relevant industrial research to investigate a new catalyst for oxidation of glycolaldehyde without these drawbacks. A catalytic process for the oxidation of

View Article Online
DOI: 10.1039/D6CY00352D



glycolaldehyde to glycolic acid using heterogeneous platinum/palladium catalyst on activated carbon or alumina supports, using air at atmospheric pressure was reported.[9] Due to the mild reaction conditions low leaching of the active metal was observed. In another patent, supported catalysts containing Pt, Pd, Ru and Rh group were used. It was claimed that the supported metallic catalyst is more active than the catalysts used in prior art and is more stable at oxygen rich conditions.[10] According to the inventors, platinum on activated carbon (Pt/C) is a promising catalyst for the glycolaldehyde oxidation to glycolic acid. Activated carbon provides a high surface area for Pt dispersion and stabilization.[12-14] The catalytic oxidation of glycolaldehyde to glycolic acid starting from ethylene glycol in presence of various $Pt_n$ clusters was discussed in a recent theoretical study.[15] Direct oxidation of glycolaldehyde to glycolic acid on Pt/C was also addressed in an experimental study.[16] While Previous studies have demonstrated the feasibility of converting glycolaldehyde to value-added products such as glycolic acid, the underlying reaction mechanisms remain incompletely understood. In particular, there is limited mechanistic insight into the factors governing selectivity, catalyst deactivation, and byproduct formation under realistic reaction conditions. Existing literature primary focus on overall conversion and selectivity trends, with comparatively less attention paid to the interplay between reaction kinetics and thermodynamics. In addition, the role of carbon support and non-catalytic (blank) contributions to the observed reactivity are highlighted in this work. Furthermore, the mechanistic pathways leading to minor byproducts, such as glyoxylic acid hydrate and oxalic acid, were not fully resolved, particularly with respect to their energetic feasibility. In this work, we address these gaps by combining experimental observations with mechanistic analysis to elucidate the reaction network over Pt/C catalyst. This integrated approach provides a more comprehensive understanding of the catalytic system and helps rationalize the observed performance limitations at elevated substrate and product concentrations. DFT-metadynamics (DFT-MTD) simulations were used to analyze the main reaction and potential side- and consecutive pathways in more detail.

Given our interest in developing biobased building blocks and biodegradable polymers[17-19], as well as our experience in catalytic oxidation of carbohydrates[20,21], we were motivated to continue the development of catalytic glycol aldehyde oxidation. While earlier reports showed that e.g. in the case of hexose or uronic acid oxidation often supported gold catalysts gave superior performance compared to platinum[17,19,20], apparently in the case of glycolaldehyde the latter was sufficiently effective. This raises the question why platinum on carbon is an efficient and selective catalyst in

View Article Online
DOI: 10.1039/D6CY00352D





this reaction. In order to gain more insights, we investigated this reaction by combining experimental work, design of experiment and DFT calculations. Here we report that under optimized reaction conditions high conversions and selectivities can be obtained using a Pt/C catalyst. Variation of substrate concentration and substrate to catalyst ratio, as well as control experiments with the main products and potential by-products and consecutive intermediates shows that the intended product (glycolic acid ) is stable, while consecutive products are quickly converted to gaseous products, yielding clean product mixtures. A suggested reaction network is presented based on the combined experimental and computational results. The outcome of this work can pave the way in utilizing bio-based resources and agricultural residues to obtain bio-glycolic acid.

**Pt on carbon (Pt/C) catalyst structure**

For the periodic DFT simulations a $Pt_4$/C molecular structure was considered as the heterogeneous catalyst that is studied in many of previous theoretical and experimental works. [15,16,22-26] Four Pt atoms make a tetrahedral cluster which is located on the carbon surface with a periodic hexagonal unit cell (a=b= 14.82 Å, c= 27.16 Å and α=ß= 90˚, γ=120˚). According to the previous studies, there are a few advantages of $Pt_4$/C over bulk Pt including higher catalytic activity (more active sites per Pt atoms) and enhanced stability (strong Pt-C interactions prevent agglomeration). The higher catalytic activity and stability of $Pt_4$ cluster have been addressed in several studies. Previous DFT calculations showed that $Pt_4$/C is more reactive for reactions that require dissociation of bonds because of the higher number of under-coordinated atoms.[24-27] Formation of the covalent bonds between the bottom Pt atom and neighboring C atoms results in a strong interaction between the $Pt_4$ cluster and the six-membered ring (C6 in short) carbon support. These interactions between Pt-C can modify the electronic properties in both atom types. The electronic properties of Pt make it highly effective for oxidation and reduction processes. The activated carbon support stabilizes Pt nanoparticles, preventing aggregation and maintaining long-term activity. Furthermore, the carbon support influences the electronic properties of Pt and tuning its catalytic behavior.[28-31] Hence, the Pt cluster can be formed and is sufficiently stable over the molecular dynamic (MD) trajectories. According to previous studies, due to the strong coordination between Pt and the carbon support, the six-membered ring structure of the activated carbon is deformed and pulled away from the horizontal plane and this affects the electronic properties of the C6 support. Overall, the strong

View Article Online
DOI: 10.1039/D6CY00352D





interactions between the Lewis acidic Pt centers, which are not bound to other atoms such as O in metal oxides, and the functional groups such as HC=O and OH in organic molecules are the driving force for bond cleavage and formation on the Pt catalyst.[32-33]

## Experimental

*General procedure for the oxidation of glycolaldehyde dimer using the Parr Reactor*

Batch experiments were performed in 75 mL Parr MRS5000 reactors which were charged with glycolaldehyde dimer, demineralized water (20 mL), catalyst and a stirring bar. The system was closed, flushed 3 times with oxygen gas (5.0, SOL Group) and pressurized to 10 bar oxygen gas. Heating was then applied to the system and stirring at 750 rpm was started. After the desired reaction time, stirring was stopped and the reactor was removed from the heating source. When the reaction mixture reached room temperature, the system was depressurized and opened. The suspension was then filtered over a microfilter and diluted to the desired concentration for HPLC analysis. The following chemicals and reference compounds were used as received i.e. formaldehyde solution, contains 10-15 % methanol as stabilizer, 37 wt% in $H_2O$, Sigma Aldrich; formic acid, 98-100%, extra pure, Merck; Glycolaldehyde dimer (1,4-Dioxane-2,5-diol), 95%, AmBeed; glycolic acid, purum >99.0% (T), Fluka; glyoxylic acid monohydrate, 98%, Sigma Aldrich; oxalic acid, 98%, Aldrich; sulfuric acid, 98%, for analysis, Merck. Platinum, 1% on granular carbon reduced nominally 50% water wet, 4x10 Mesh, Alfa Aesar and platinum, 1wt%, matrix activated carbon support, Aldrich were used as the commercial catalysts. Prior to use, the water wet catalyst was pre-dried at 120 °C for 1 h and crushed in a mortar to give a fine powder.

**Catalyst recycling experiments**

Batch recycling experiments were performed in 75 mL Parr MRS5000 reactors which were charged with glycolaldehyde dimer (200 mg), demineralized water (20 mL), Pt/C (1wt%, 100 mg) and a magnetic stirring bar. In the first run, six parallel experiments were performed using the fresh catalyst. After following the general procedure, including individual HPLC analysis of each separate reactor, the catalysts from each series were pooled, collected by filtration over a paper filter, washed with water, dried at 120 °C, and reused in the consecutive runs. For the second run, five parallel reactions were performed using the catalyst recovered from run one. For the third run, four parallel reactions were performed with the recovered catalyst from run two, and so on. The catalyst after run four was collected for further analysis and characterization.

**Analytical methods**

View Article Online
DOI: 10.1039/D6CY00352D



HPLC analyses were performed on a Waters e2695 HPLC instrument, equipped with a Concise Corogel Ion 300 (30 cm length) column, maintained at 65 °C, using $H_2SO_4$ (3 mM) in MilliQ water as the eluent, with a flow rate of 0.4 mL $min^{-1}$. The components were identified using a Waters 2489 UV/Vis Detector (210 nm) and a Waters 2414 RI detector. An overview of all HPLC spectra as well as calibration plots and replication errors are displayed in SI **Figure S1 A-E**.

**Elemental analysis**

The Pt-loading of the catalysts and dissolved Pt-concentrations were determined externally by Mikroanalytisches Laboratorium Kolbe, Oberhausen, Germany. The catalyst samples were dried for 1h at 120 °C at 10 mbar pressure prior to analysis, and the liquid samples were filtered over a 45 μm filter. Analysis was performed in duplicate.

**$N_2$-Physisorption**

$N_2$ adsorption-desorption isotherms at -196 ˚C were measured using a Micromeritics TriStar II Plus. The Pt/C catalyst samples were pre-dried at 120 ˚C for 1 h, and 0.1-0.2 g of sample was used for the measurement. The sample was outgassed for 20 h under vacuum (< 0.1 mbar) at 200 ˚C prior to measurement. The linear part of the BET equation (relative pressure between 0.05 and 0.30) was used for the determination of the specific surface area. The microporous pore volume was determined using the *t*-plot method. The pore size distribution was calculated from the adsorption branch of the $N_2$ physisorption isotherms and the Barret–Joyner–Halenda (BJH) formula from BET (4V/A). The results are shown in Table 5.[21]

**Scanning transmission electron microscopy (STEM)**

Scanning transmission electron microscopy (STEM) measurements were conducted on a Titan aberration-corrected Transmission Electron Microscope operating at 300kV with a point-to-point spatial resolution of 0.12nm in STEM mode equipped with a CETA 16M camera and ChemiSTEM system for energy-dispersive X-ray spectroscopy (EDX) chemical compositional analysis. Before measurements, Pt/C samples were finally powdered and dispersed in ethanol. A small droplet of this dispersion was deposited onto a carbon coated copper grid.

**X-ray Photoelectron Spectroscopy (XPS)**

X-ray Photoelectron Spectroscopy (XPS) data were acquired using a SPECS GmbH system equipped with a PHOIBOS 150 9MCD hemispherical energy analyzer. A non-monochromatic Mg X-ray source, operating at 200 W and 12 kV, was employed for the analysis. Samples were initially placed in a pre-treatment chamber at room temperature and degassed for several hours before their

View Article Online
DOI: 10.1039/D6CY00352D

subsequent transfer to the analysis chamber. Pass energies of 50 eV and 20 eV were utilized for the acquisition of survey and high-resolution spectra, respectively.

## Computational methods

To simulate the heterogeneous $Pt_4$/C molecular system, periodic *ab initio* molecular dynamics calculations (DFT-MD) were used. Periodic DFT calculations were performed using unit cell parameters highlight the inherent solid (heterogeneous) phase of the catalyst. The periodic model reproduces the unit cell through space, effectively representing heterogeneous phase.[24,27] In this model the single unit cell is replicated throughout the 3D space. As such, the model simulates the large crystal structure. Water molecules, substrates, Pt4 are continuously replicated within the periodic boundary conditions. Carbon support was modeled as pristine graphene, and no additional heterogeneity such as defects, dopants, or surface functional groups was explicitly included. All periodic DFT calculations – including geometry optimizations and *ab initio* molecular dynamics (AIMD) simulations – were performed using CP2K software package with the Gaussian and plane-wave (GPW) method.[34] The valence orbitals were expanded in the DZVP-MOLOPT Gaussian basis set[34] in combination with Goedecker, Teter and Hutter pseudopotentials were used with a plane wave cutoff energy of 400 Ry.[35] We used the PBE density functional,[36] also augmented with Grimme D3 dispersion correction.[37] The criteria for self-consistent field (SCF) convergence were set to $5.0\times10^{-7}$ and for the calculated free energy values to $1.0\times10^{-9}$ kcal/mol. Four Pt atoms make a tetrahedral cluster which is located on the carbon surface with a periodic hexagonal unit cell (a=b= 14.82 Å, c= 27.16 Å and α=ß= 90˚, γ=120˚). The AIMD simulations were performed in an NVT ensemble, with the temperature controlled by a canonical sampling through velocity rescaling (CSVR) thermostat, set at a temperature of 343 K, and a period of 500 fs. The MD time step was set to 0.5 fs. To investigate the reaction mechanism at finite temperature, elucidate the reaction pathway and identify the transition state region between reactant and product states, we performed metadynamics (MTD) simulations using the PLUMED plug-in in combination with CP2K.[38-40] Metadynamics simulations explore free energy landscapes and identify optimal pathways in the presence of all reactant molecules and catalyst. The key role of metadynamics simulation in revealing the main and side elementary steps of complex reactions are discussed in plenty of recent literature.[41-45] The simulations were initiated from the optimized molecular structures (obtained by static DFT calculations) and conducted until several transition state re-crossing events could be observed. To prevent sampling from unnecessary regions of the FES,


View Article Online
DOI: 10.1039/D6CY00352D



harmonic walls with a force constant K = 250 kcal/molÅ$^2$ were used for the collective variables (CVs), with the Gaussian bias potentials added every 25 steps. Six water molecules and one $^3O_2$ are explicitly included in the system in addition to the substrate molecules and Pt/C catalyst. Multiple test simulations were run to set the computational parameters, including the height and width of the Gaussian bias potentials and the quadratic walls. The CVs for each reaction step are correlated to the relevant distances which are depicted in the proposed mechanism for each step. Using the trace_irc code structures of the minima and the transition states were refined.[45,46] The structures of reactant, transition state, and product complexes are shown in SI with selected distances (Å). Visualization of the MD trajectories and individual snapshots, we used the VMD software package.[47,48]

## Results and Discussion

The catalytic oxidation of glycolaldehyde to glycolic acid starting from ethylene glycol in presence of $Pt_n$ clusters as well as direct oxidation of glycolaldehyde to glycolic acid on Pt on carbon support have been recently addressed in literature theoretically and experimentally.[15,16] However, in the experimental study the applied reaction conditions were under 25 bar $O_2$ pressure and 30 ˚C while in this work we use 10 bar $O_2$ pressure and 70 ˚C. In addition, in this work the possible consecutive side pathways are analyzed both experimentally and using DFT calculations, which were not reported in the previous studies. In a recent theoretical work,[16] the authors discussed different cluster sizes of $Pt_n$ catalyst but not on the carbon support. Herein, we address all the calculations (main and side/consecutive paths) at 70 ˚C using AIMD simulations on Pt/C. Furthermore, the commercially available glycolaldehyde dimer can exist via equilibria in several shapes in aqueous solution and low concentration, which we discuss them later in this work.[49-51] Herein, as the preliminary reaction conditions, the oxidation of glycolaldehyde was tested with a (powdered) granular 1 wt% Pt/C catalyst. The initial screening experiments were performed at different temperatures (80 – 100 – 120 °C) for 4 h, and the results are summarized in Table 1. It was observed that with increasing reaction temperature the conversion of glycolaldehyde increases, while the carbon balance decreases. Furthermore, the selectivity to glycolic acid decreases with increasing reaction temperature. At 60 ˚C the conversion and selectivity are very high, combined with an almost quantitative carbon balance which shows that Pt/C is a promising catalyst.

View Article Online
DOI: 10.1039/D6CY00352D



**Table 1.** Variation of conversion, selectivity and carbon balance vs. temperature in conversion of glycolaldehyde to glycolic acid in the presence of Pt/C catalyst. Preliminary test reaction conditions: 1wt% substrate concentration in 20 mL water, 100 mg 1wt% Pt/C (0.32 mEq Pt), 4 h, 10 bar oxygen, stirring at 750 rpm.

| Entry | Temp. (°C) | Conversion (mol%) | Glycolic acid sel. (mol%) | Carbon balance (mol%) |
|---|---|---|---|---|
| **1** | 60 | 87 | 95 | 99 |
| **2** | 80 | 94 | 91 | 94 |
| **3** | 100 | 97 | 68 | 69 |

**Design of Experiment (DoE) analysis and results**

To investigate the critical reaction parameters and optimize the glycolic acid yield, a design of experiment (DoE) was performed using the 1wt% Pt/C catalyst at a fixed 0.32 mEq Pt/substrate ratio, a fixed 1 wt% glycolaldehyde concentration, and an oxygen pressure of 10 bar. For practical reasons (as well as equipment limitations), the input variables for the DoE were a temperature window of 40 to 80 °C and a time window of 0.5 to 8 h. Next, a central composite design was created, resulting in 12 design points/experiments. These experiments were randomized and performed according to the design points. The response (glycolic acid yield in mol%) was determined by HPLC analysis. An overview of the 12 experiments (variables and response) is shown in **Table S1** in SI. Based on these data, a previously reported DoE method was used to fit the best response surface.[52]

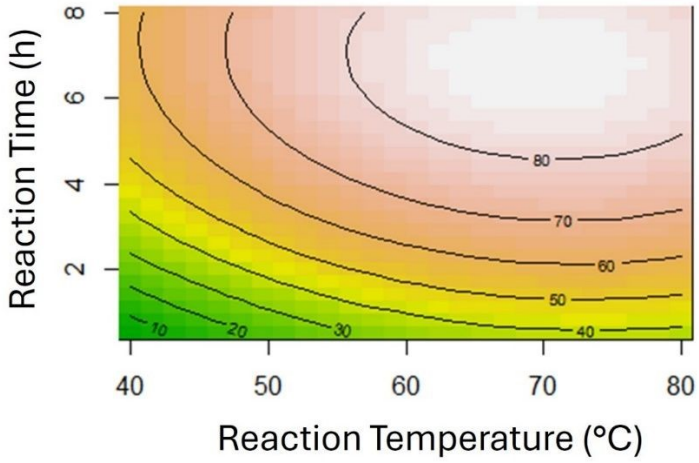

View Article Online
DOI: 10.1039/D6CY00352D

**Figure 1.** Graphical representation of the predicted glycolic acid yield (mol%) depending on the two considered variables, i.e., reaction temperature and reaction time.

The model has a high statistical significance (p-value = 0.000445) and good coefficient of determination ($R^2$ = 0.959), indicating that the model describes the data well. Figure 1 is a graphical representation of the model, showing the predicted glycolic acid yield depending on reaction temperature and reaction time. The highest predicted yield of glycolic acid is 86 mol% at an optimal temperature of 70 °C and a reaction time of 7 h. Next, experiments were performed according to the predicted optimal reaction conditions. This resulted in a glycolic acid yield of 95 mol%, which is superior to the prediction (Table 2, entry 1).

**Control experiments: stability of reagent and (side)products**

Additional control experiments were performed to evaluate the stability of glycolic acid and possible by-products and consecutive products under the predicted optimal reaction conditions (70 ˚C and 7 h). The results are summarized in **Table 2**. It was observed that the desired product, glycolic acid, was quite stable: only 3 mol% was converted into glyoxylic acid and oxalic acid, and potentially into volatile gases like $CO_2$. (Table 2, entry 2). The (expected) side-products all showed very low stability under the reaction conditions, as almost full conversion was observed for glyoxylic acid, oxalic acid, formic acid, glyoxal and formaldehyde (Table 2, entries 3-7).

The observed glyoxylic acid in the stability test of glycolic acid (Table 2, entry 2) seems at contrast with the almost complete decomposition of glyoxylic acid itself (Table 2, entry 3). However, the pure glycolic acid mixture has a high acidity, and due to the slow conversion (given the stability of glycolic acid), the pH stays low throughout the reaction. A low pH is known from literature to slow down the conversion on Pt/C catalyst. Therefore, once glyoxylic acid is formed from glycolic acid, it is only slowly converted because of the acidic medium and can be observed.

Starting from glyoxylic acid, which by itself is not a stable compound, the reaction mixture also starts acidic. But the more glyoxylic acid decomposes, the less acidic the mixture becomes, and the faster the conversion will go, thereby explaining the almost full conversion. The same is the case for formic acid and oxalic acid: decomposition leads to a less acidic reaction mixture.

Based on these experimental observations, it can be concluded that glycolic acid is the most stable product, while the side products (glyoxylic acid, oxalic acid, formic acid, glyoxal and

View Article Online
DOI: 10.1039/D6CY00352D



formaldehyde) easily decompose. Also, the fast decomposition of potential side products might be beneficial for downstream processing of the product mixture. This makes Pt/C a very promising catalyst for the conversion of glycolaldehyde, given the very high selectivity to glycolic acid. A further explanation for these observations will be supported by DFT calculations, later in this paper.

**Table 2.** Control experiments and stability of (side) products under optimal reaction conditions: 1wt% substrate concentration in 20 mL water, 100 mg 1wt% Pt/C (0.32 mEq Pt), 70 ˚C, 7 h, 10 bar oxygen, stirring at 750 rpm.

| Entry | Substrate | Conversion (mol%) | Glycolic acid sel. (mol%) | Glyoxylic acid sel. (mol%) | Oxalic acid sel. (mol%) | Carbon balance (mol%) |
|---|---|---|---|---|---|---|
| **1** | Glycolaldehyde[a] | 95 | 99 | 0.4 | | 99 |
| **2** | Glycolic acid[a] | 3.2 | | 2.8 | 0.2 | 97 |
| **3** | Glyoxylic acid[a] | 99 | | | | 0.5 |
| **4** | Oxalic acid[a] | 100 | | | | 0 |
| **5** | Formic acid[a] | 100 | | | | 0 |
| **6** | Glyoxal[a] | 100 | | | | 0 |
| **7** | Formaldehyde[b] | 96 | | | | 4 |

*[a]: granular crushed; [b]: powder catalyst*

**Effect of substrate concentration and catalyst concentration**

Next, the effect of glycolaldehyde substrate concentration and amount of catalyst was investigated. First, at 1 wt% glycolaldehyde concentration, the ratio of Pt-catalyst to substrate was increased in three steps (Table 3, entries 1-3). With increasing catalyst to substrate ratio, the glycolaldehyde conversion also increased from 68% to 91%, and even full conversion at the highest ratio. The selectivity towards glycolic acid and the carbon balance were almost quantitative at the lowest catalyst loading (Table 3, entry 1). When the amount of catalyst was increased, selectivity and carbon balance both decreased (Table 3, entries 2-3). This indicates that despite the previously observed high stability of glycolic acid, at very high catalyst concentrations glycolic acid can still slowly undergo further conversion.

View Article Online
DOI: 10.1039/D6CY00352D

**Table 3.** Influence of substrate and catalyst concentration: Variable substrate concentration in 20 mL water, varying amount of 1wt% Pt/C, 70 ˚C, 2 h, 10 bar oxygen, stirring at 750 rpm.

| Entry | Substrate conc. (wt%) | Pt/substrate ratio (mEq) | Conv. (mol%) | Glycolic acid sel. (mol%) | Glyoxylic acid sel. (mol%) | Carbon balance (mol%) |
|---|---|---|---|---|---|---|
| 1 | 1 | 3.2 | 68 | 100 | 0.7 | 101 |
| 2 | 1 | 9.6 | 91 | 93 | 1.5 | 95 |
| 3 | 1 | 25.6 | 100 | 58 | 0 | 58 |
| 4 | 5 | 0.64 | 16 | 100 | 0 | 103 |
| 5 | 5 | 3.2 | 64 | 95 | 2.8 | 98 |
| 6 | 10 | 0.32 | 7 | 100 | 0 | 101 |
| 7 | 10 | 3.2 | 26 | 81 | 0 | 95 |

HPLC chromatograms corresponding to the **Table 3** entries are provided in the SI **Figure S1B**. Next, the substrate concentration was increased from 1 wt% to 5 wt%. Comparison of **Table 3** entries 1 and 4 shows the effect of increased substrate concentration, while the absolute amount of catalyst was kept identical (Note: as a result, the Pt/Substrate ratio also drops by an equal factor of 5: 3.2 mEq./5 = 0.64 mEq.) This resulted in a lower conversion of glycolaldehyde, from 68 mol% to 16 mol, while the selectivity towards glycolic acid and the carbon balance were not affected (Table 3, entries 1 and 4). The decrease in conversion was approx. a factor of 5 and can thus be explained by the 5x lower Pt/substrate ratio. A further increase in concentration to 10%, (Table 3, entry 6) still resulted in excellent selectivity and carbon balance, while a ~10x drop in conversion was observed, again in line with expectations.

Increasing the substrate concentration from 1wt% to 5wt% while keeping the Pt/ substrate ratio the same (Table 3, entries 1 and 5): resulted in a slight drop in conversion (from 68% to 64%), selectivity (from 100% to 95%) and mass balance (from 101 to 98%). However, when the substrate concentration was further increased to 10 wt% (again with an identical Pt/substrate ratio), the conversion dropped to 26%, the selectivity towards glycolic acid dropped to 81%, and a carbon balance of 95% was obtained. (Compare Table 3, entries 1, 5 and 7) This result contrasts with expectations, as increased substrate and catalyst concentrations typically should result in faster mass transfer and thus higher conversion. One potential explanation might be that the increased substrate concentration results in different equilibria between glycolaldehyde dimer, open forms and hydrates. As the reaction at higher concentration requires more oxygen, gas-liquid oxygen transfer limitations might also play a role. Another possible explanation might be that the formed


View Article Online
DOI: 10.1039/D6CY00352D





glycolic acid slows down the reaction, due to pH effects and/or competitive adsorption at the Pt surface (product inhibition). These possible explanations will be quantitatively discussed in the next part with the aid of DFT calculations.

**Simulation of glycolaldehyde to glycolic acid conversion and consecutive side pathways**

Using static DFT calculations the possible equilibria between glycolaldehyde dimer and monomer in a diluted aqueous solution were investigated. According to literature[49-51], pure glycolaldehyde that is commercially available in its cyclic dimer form undergoes equilibrium transformations upon dissolution in water and generates various molecular species upon interaction with the environment, which is aqueous neutral (literature) and neutral to acidic (in this study, i.e., oxidation to glycolic acid). In **Scheme 1** we have depicted the equilibrium species based on the reactions of the glycolaldehyde dimer in water.[49]

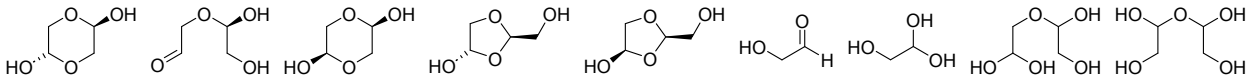


**Scheme 1.** Schematic representation of various species produced upon interaction of glycolaldehyde dimer (commercially available) with water in aqueous solution.

The energetics of formation of the species depicted in **Scheme 1** (were calculated using explicit water molecules in Ref. 47) are reported in **Table S2** in SI . For comparison, we calculated the energetics including a mixture of explicit glycolic acid and water molecules (three $H_2O$ and three glycolic acid) and the values of $\Delta G$ and $\Delta G^{\neq}$ are reported in **Table S2** in SI. Explicit glycolic acid as well as water molecules in the calculation of the equilibria were included since glycolic acid is formed continuously during the oxidation reaction. According to these results, hydrolysis of cyclic glycolaldehyde dimer (**1**) to linear glycolaldehyde dimer (**2**) is a thermodynamically favorable and kinetically not very demanding transformation. The cyclic rearrangements of **2** to **3**, **4** and **5** are unfavorable thermodynamically with higher barriers than **1** to **2**. Production of glycolaldehyde monomer by hydrolysis of the dimer (entry **5**) has the most favorable thermodynamics and rather favorable kinetics and therefore is the most dominant equilibrium amongst the others. This implies that in a dilute aqueous solution the dimer is not stable and hydrolyses to the monomer. Formation of glycolaldehyde monomer is followed by a nucleophilic attack by a water molecule on the carbonyl, forming the glycolaldehyde hydrate that is slightly less favorable transformation thermodynamically (0.66 and 1.45 kcal/mol in neutral and acidic environments, respectively),

View Article Online
DOI: 10.1039/D6CY00352D



however, this slightly positive ΔG can be compensated considering that water molecules are omnipresent in the reaction environment and kinetically the barrier for water attack is not very high at room temperature (16.05 and 15.45 kcal/mol, in explicit water and explicit water and glycolic acid, respectively). We note that previous NMR and FTIR studies reported in literature identified (at room temperature in $D_2O$) the presence of at least four molecular species, in which the predominant observed species in the mixture was the hydrate form (**7**) of glycolaldehyde (70%, shown in **Scheme S2** in SI).[52,53]

**Oxidation of glycolaldehyde to glycolic acid**

**I. Glycolaldehyde to glycolic acid**

**Figure 2** shows the proposed mechanism for oxidation of glycolaldehyde (GAL) which consists of a $H^-$ transfer to the Lewis acidic Pt followed by a nucleophilic attack by $H_2O$ from the surrounding environment. Hence, the weak nucleophilic attack by $H_2O$ is triggered by a preceding $H^-$ transfer to the Pt and generation of partially positive charge on the C(C=O). This can be observed in **Figure 2B** that the bond formation between H···Pt takes place earlier than $H_2O$···C(C=O).

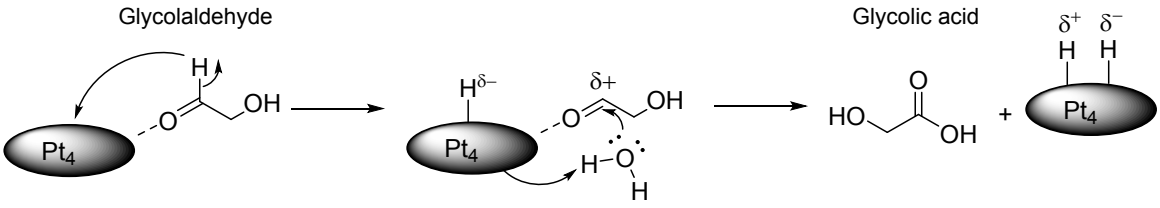


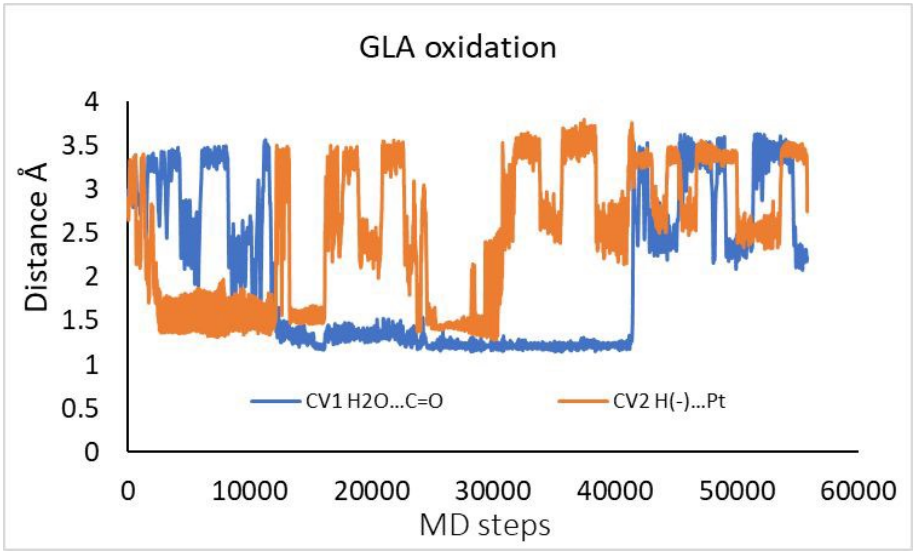

View Article Online
DOI: 10.1039/D6CY00352D



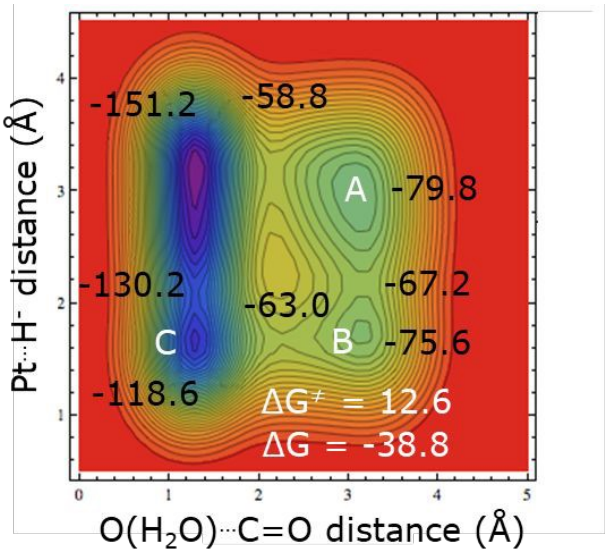


**Figure 2.** Oxidation of glycolaldehyde; **A)** proposed mechanism, **B)** variation of the CVs; **C)** calculated FES, the numbers show Gibbs free energies in kcal/mol.

This reaction is thermodynamically strongly exergonic (ΔG of -38.8 kcal/mol with a barrier of 12.6 kcal/mol). After formation of glycolic acid, the acidic $H^+$ (COOH) leaves the molecule and as can be seen in **Figure 3** attaches to various Pt atoms for specific time intervals (the Pt···$H^+$ distance of 1.6 – 1.8 Å). This $H^+$···Pt bond formation can temporarily block the $Pt_4$. This explains the experimental observation related to the lower conversion of GAl→ GAc in an acidic reaction environment, which is due to the blocked catalyst by $H^+$ from acidic environment. The hydrogenated Pt catalyst is oxidized by interaction with $O_2$ in the reaction atmosphere and Pt(0) is regenerated by formation of $H_2O_2$ which is discussed later in this work.

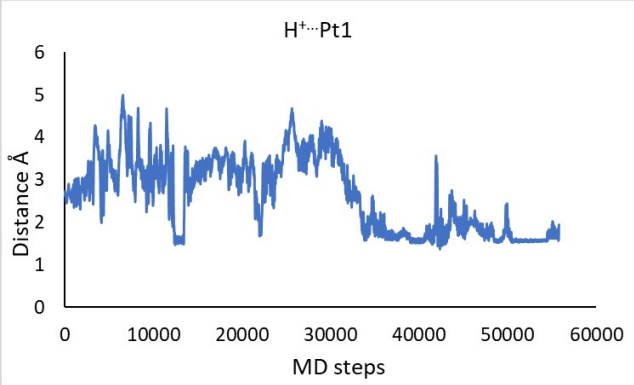

View Article Online
DOI: 10.1039/D6CY00352D



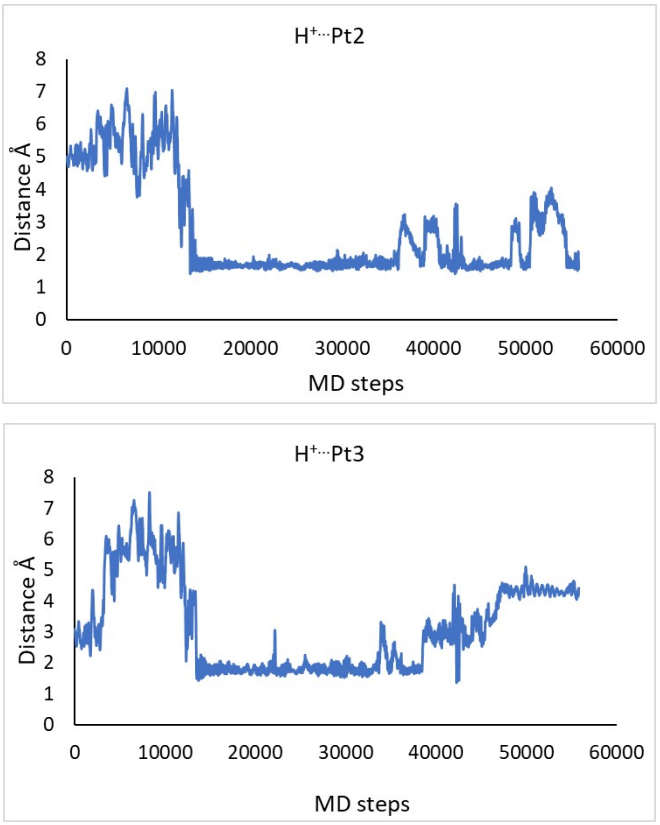


**Figure 3.** Various (glycolic acid)$H^{+}\cdots$Pt distances after generation of glycolic acid.

## II. Glycolaldehyde hydrate to glycolic acid

**Figure 4** shows details of oxidation of hydrate form of glycolaldehyde . The proposed mechanism (**4A**) starts with a $H^-$ transfer to Pt which is followed by a $H^+$ abstraction by a water molecule in the proximity and generation of a hydronium ion. The $H^-$ transfer occurs earlier than $H^+$ abstraction according to the variation of CVs against the reaction steps (**4B**). The barrier of this transformation is 4.8 kcal/mol and the reaction is quite exergonic (ΔG of -48.6) similar to the glycolaldehyde monomer oxidation. The lower barrier of oxidation in case of glycolaldehyde hydrate is in line with higher conversion rate at lower concentrations of glycolaldehyde in experiment that confirms predominant portion of glycolaldehyde in hydrate form. As shown in **Figures 2** and **4** the $H^-$ transfer to the Pt catalyst is an energetically favorable step that assists the $H^+$ abstract. This means that enough Lewis acidity of the Pt enables the $H^-$ transfer. In the glycolaldehyde hydrate pathway and after formation of the $H3O^+$ ion as a medium intermediate (similar to glycolic acid) the $H^+$ transfers to the Pt catalyst. Hence, during the reaction both $H^-$ and $H^+$ bind to the catalyst forming platinum hydride. The Pt bound $H^{-}\cdots{}^{+}H$ is subsequently transferred to molecular oxygen, forming $H_2O_2$ and Pt(0), thereby reactivating the catalyst. The complete reaction between oxygen and $H^-$/

View Article Online
DOI: 10.1039/D6CY00352D



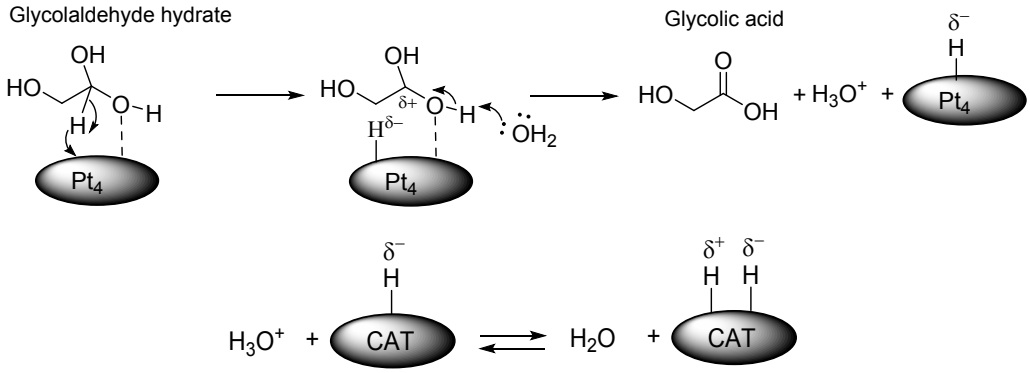


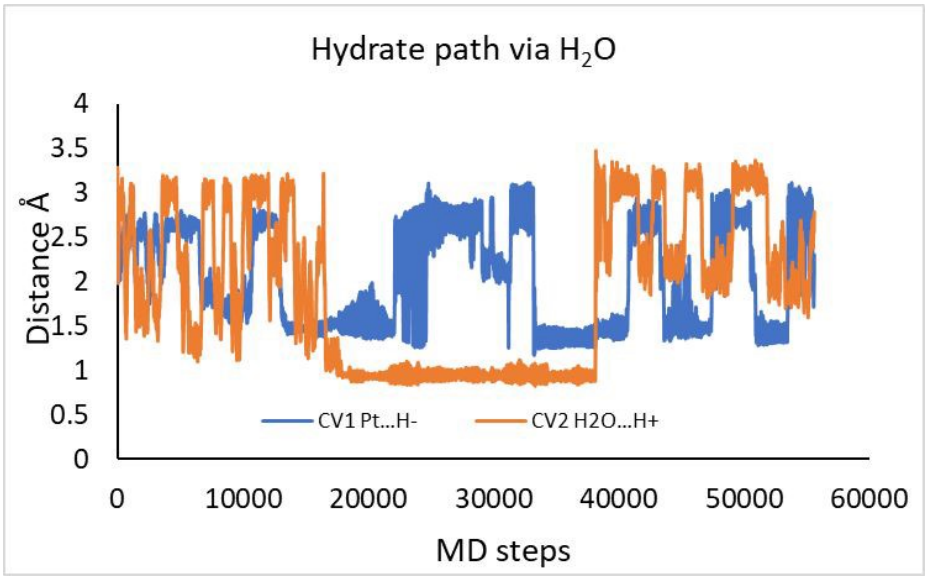


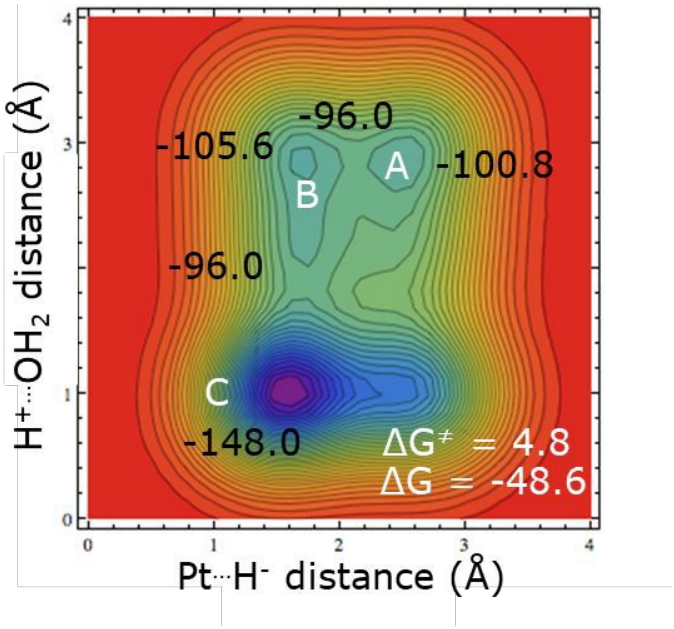

View Article Online
DOI: 10.1039/D6CY00352D

**Figure 4.** Oxidation of glycolaldehyde hydrate; **A)** proposed mechanism, **B)** variation of the CVs; **C)** calculated FES, the numbers show Gibbs free energies in kcal/mol.

$H^+$ is discussed later in the paper. In summary, the hydrate is more reactive than the free aldehyde, and there is a dynamic equilibrium between aldehyde and hydrate, hence, the glycolaldehyde hydrate path is the kinetic route and hydrate reacts faster and pulls aldehyde through equilibrium.

**Stability of glycolic acid and consecutive side products**

Alongside the main oxidation reaction of glycolaldehyde, which according to the simulated FESs has rather favorable kinetics and thermodynamics, some consecutive side reactions are also feasible in the reaction network that produce consecutive side products . Here, the stability of glycolic acid against further oxidation of the alcohol group and conversion to glyoxylic acid is investigated. **Figure 5A** shows our proposed mechanism, which is $H^-$ transfer to the Pt and $H^+$ abstraction by Pt, for dehydrogenation (oxidation) of the $CH_2OH$ functionality in glycolic acid and conversion to glyoxylic acid with the involvement of Pt atoms.

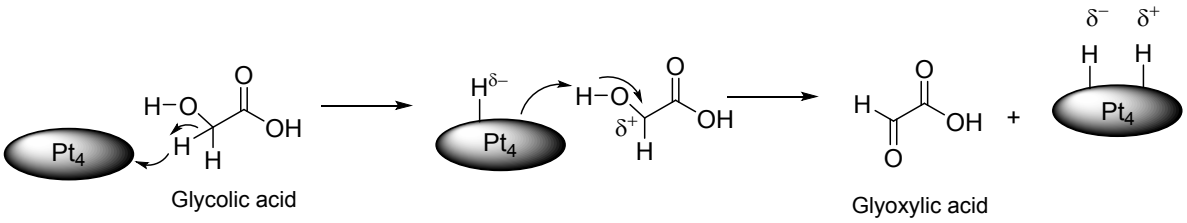


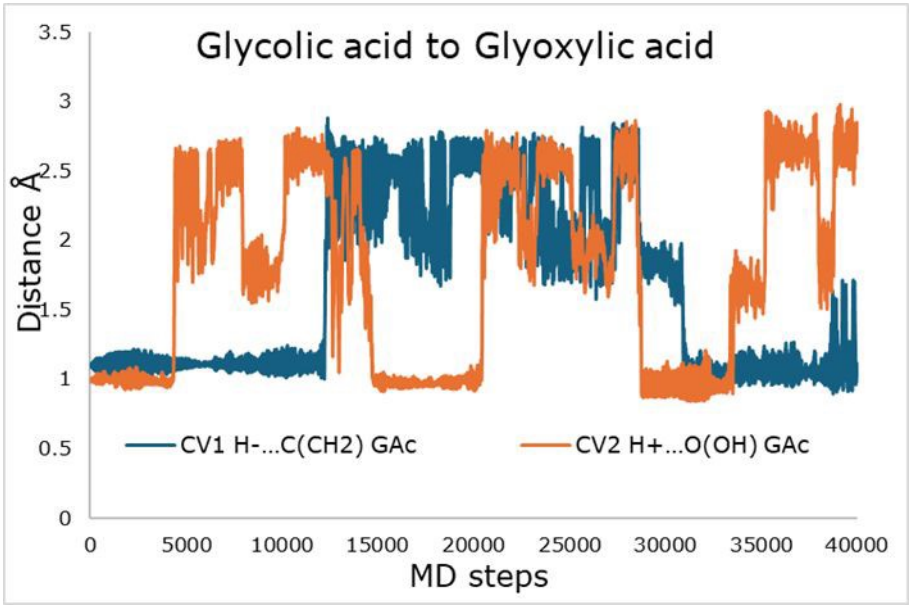

View Article Online
DOI: 10.1039/D6CY00352D



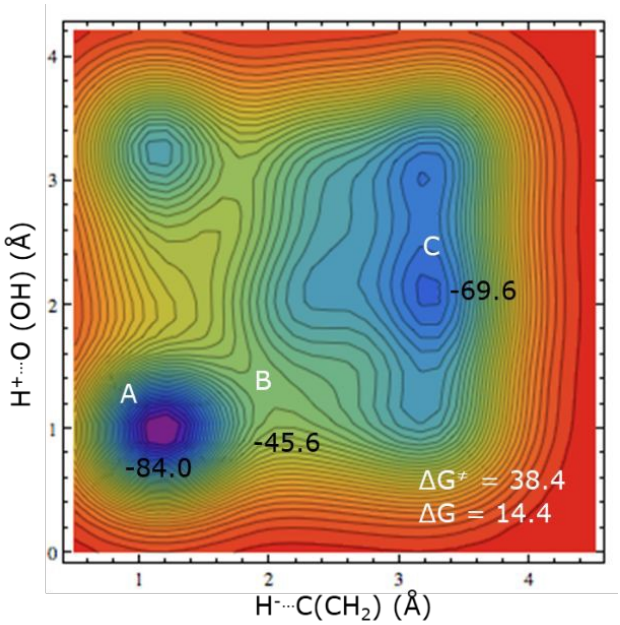


**Figure 5.** Proposed mechanism (**A**) for dehydrogenation of the $CH_2(OH)$ group in glycolic acid and conversion to glyoxylic acid with the involvement of Pt centers, **B**) variation of the CVs, **C**) simulated FES of the reaction, the numbers show Gibbs free energies in kcal/mol.

The calculated FES in **Figure 5C** indicates a barrier of 38.4 kcal/mol and the reaction free energy of 14.4 kcal/mol. The unfavorable kinetic and thermodynamic of the glycolic acid oxidation in comparison to glycolaldehyde confirms the stability of glycolic acid at the experimental reaction condition and is in agreement with the experimental observations (**Table 2**, entry 2). The stability of glycolic acid was reported in previous studies as well as industrial reports.[52,53] The acidic $H^+$ (COOH) of glyoxylic acid has a strong interaction with a nearby Pt that can be identified by probing the $H^+$···Pt distance alongside the simulated MD trajectory (**Figure 6**). The Pt-$H^+$ can cause a temporary deactivation of catalyst.

View Article Online
DOI: 10.1039/D6CY00352D

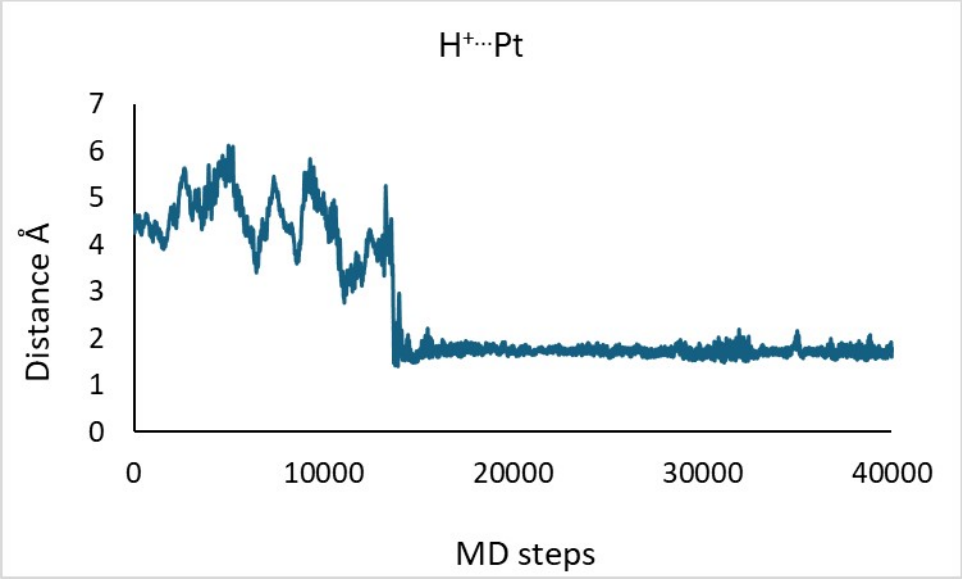


**Figure 6.** Variation of the distance between acidic $H^+$ (COOH) and Pt atom during the trajectory of glycolic acid oxidation.

The control experiments for the stability of glyoxylic and oxalic acids showed that these two side products are rather unstable and completely convert to the other compounds (99% and 100% conversions) at the same reaction conditions (**Table 2**, entries 3 and 4). To investigate these observations we performed metadynamics simulations for the conversion reaction of glyoxylic to oxalic acid as well as oxalic acid decomposition. The simulated FESs are shown in **Figure 7** with the proposed mechanisms for these transformations. Analysis of complexation of various species in the reaction mixture to the Pt atom (**Figure S3)** confirms that glyoxylic acid complexation to the Pt is the strongest interaction and results in an increase of the positive charge on C(C=O) atom. The increase of positive charge causes more electrophilic character on the carbonyl carbon of glyoxylic acid which prepares it for a nucleophilic attack by an $H_2O$ molecule in the proximity. As a quantitative indicator of catalyst deactivation the values of complexation energies between glycolaldehyde monomer, glycolaldehyde hydrate and glycolic acid with Pt center (via various functionalities) as well as variation of the electronic atomic charges of functional groups involved in complexation were listed in **Table S3** and **Figure S4** in SI. Catalyst deactivation (which is often coupled with pore diffusion inside carbon) due to substrate or product complexation in many systems is a primary cause of performance decay at high concentrations. The FES indicates a barrier of 8.0 kcal/mol and reaction free energy of -58.8 kcal/mol, which is extremely exergonic

View Article Online
DOI: 10.1039/D6CY00352D



due to decomposition of oxalic acid intermediate to small molecules. Variation of the C-C distance of glyoxylic acid alongside the MD trajectory (shown in part A-III **Figure 7**) confirms C-C bond cleavage a while after oxalic formation. This is in line with the results reported in **Table 2,** as well as industrial reports, in which glyoxylic acid directly converts to small molecules $CO_2$, CO and $H_2O$.[51,52]

Decomposition of oxalic acid through a C-C bond cleavage is depicted in **Figure 7B**. The $\Delta G^{\neq}$ and $\Delta G$ of oxalic acid decomposition are 14.5 and -13.5 kcal/mol, respectively. The carbon…Pt and O…Pt distances of COOH and Pt are depicted in **Figure 7B-III** that show strong interaction between COOH and Pt that can further decompose to formaldehyde.

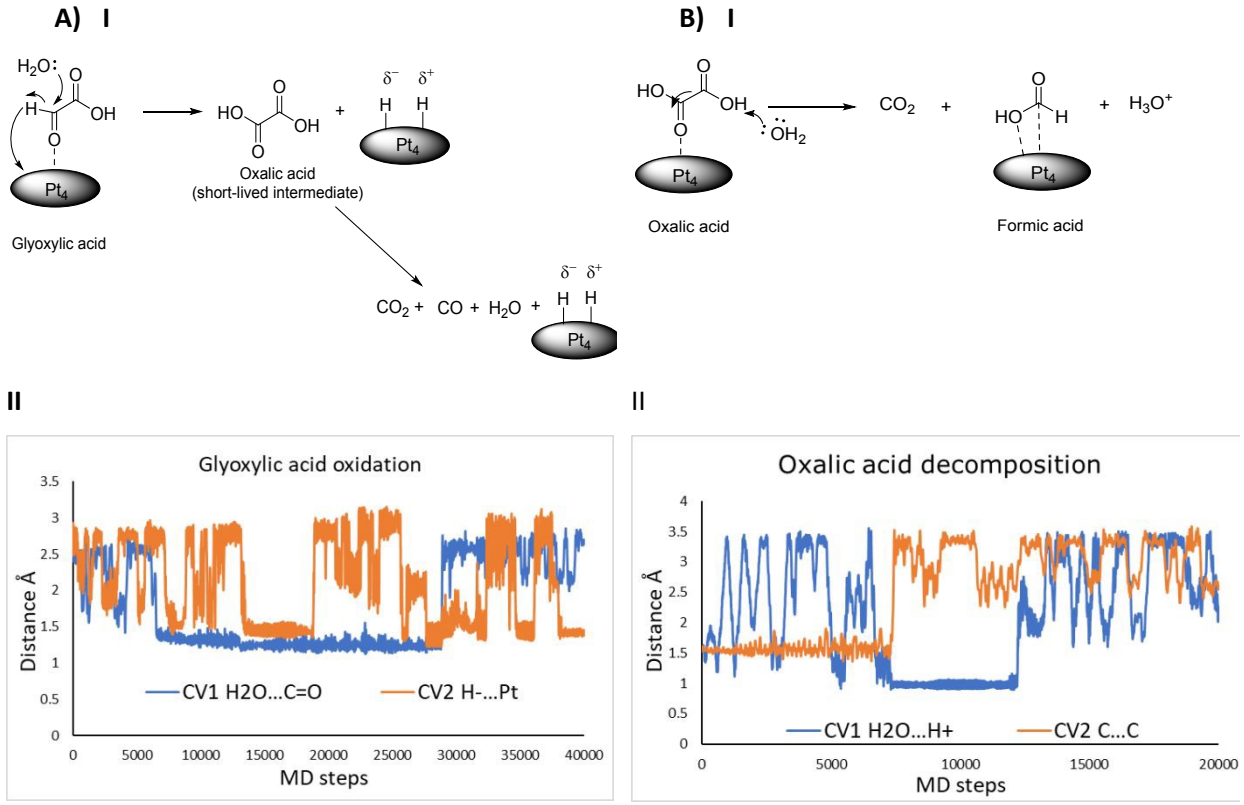

View Article Online
DOI: 10.1039/D6CY00352D



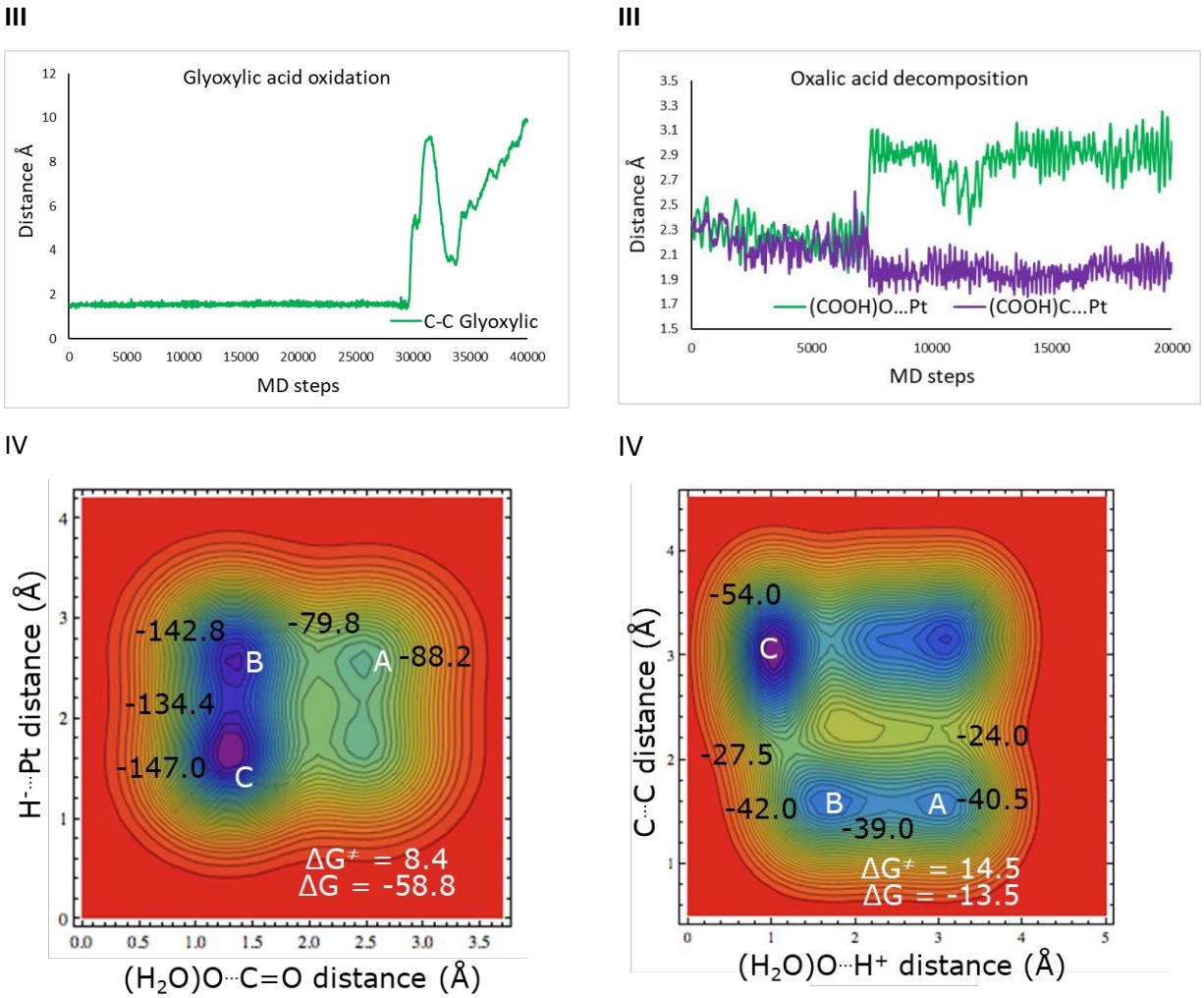


**Figure 7. A)** Transformation of Glyoxylic acid to oxalic acid and then to $CO_2$, CO, $H_2O$ and $H^+/H^-$ on Pt), **B)** Decomposition of oxalic acid to $CO_2$, formic acid and $H_3O^+$.

Alternatively, glyoxylic acid in an aqueous solution strongly interacts with water and forms glyoxylic hydrate while strong interaction between Pt catalyst and glyoxylic acid facilitates this transformation. **Figure 8A** shows conversion of glyoxylic acid to glyoxylic hydrate with a barrier of 9.0 kcal/mol and reaction free energy of -41.4 kcal/mol (strongly exergonic) and in **Figure 8B** conversion of glyoxylic hydrate to oxalic acid is shown. The later transformation is favorable as well (a barrier of 4.2 and reaction free energy of -7.0 kcal/mol).

View Article Online
DOI: 10.1039/D6CY00352D





**A)**

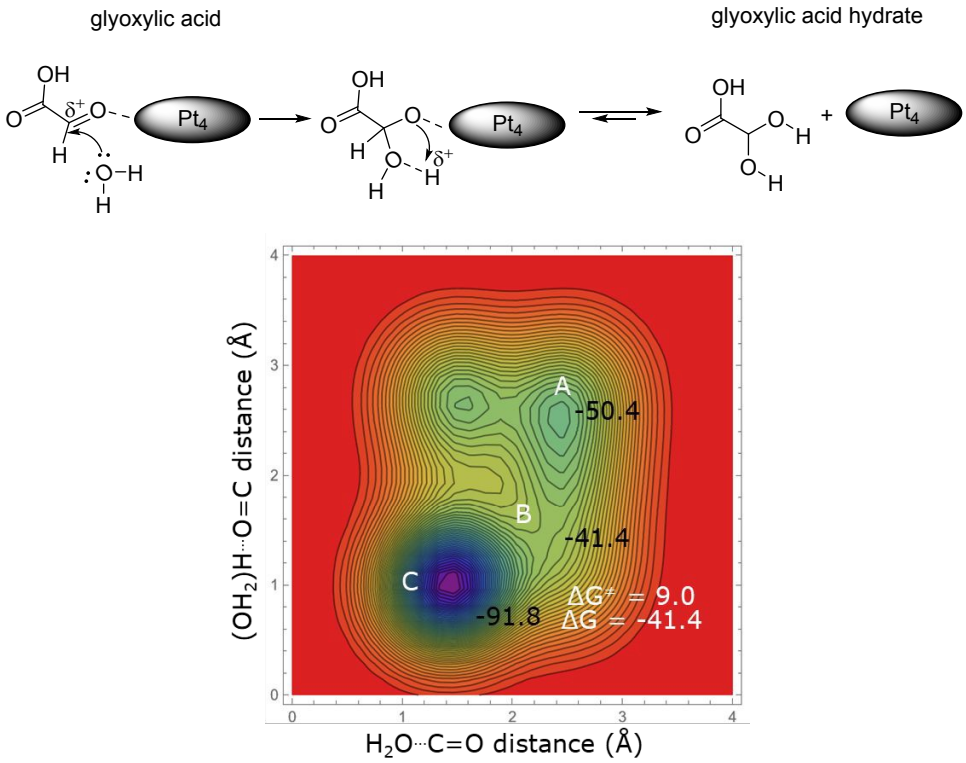


**B)**

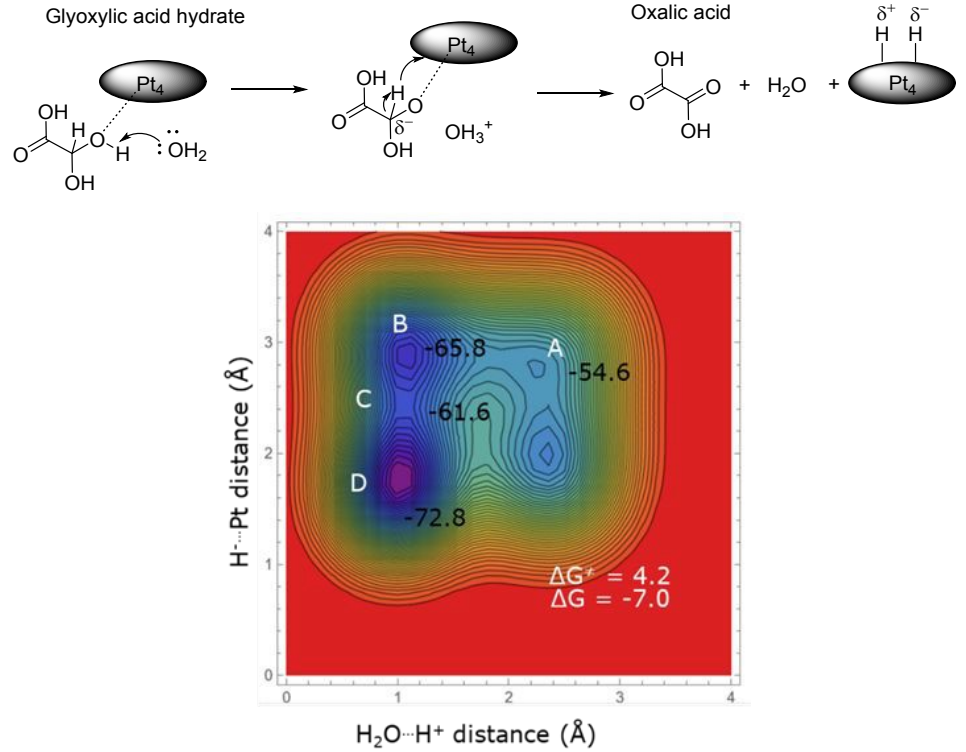


**Figure 8A. A)** Glyoxylic acid hydration to glyoxylic hydrate, **B)** Glyoxylic hydrate to oxalic acid.

View Article Online
DOI: 10.1039/D6CY00352D



The byproduct traces, glyoxylic acid and oxalic acid with 2.8 mol% and 0.2 mol%, respectively, are consecutive byproduct of glycolic acid oxidation. However, the calculated barrier of formation of glyoxylic acid is 38.4 kcal/mol which is quite higher than formation of glycolic acid from glycolaldehyde. This suggests that glycolic acid is the more stable product, and further oxidation to glyoxylic acid is kinetically hindered. Consequently, the formation of glyoxylic acid is limited, consistent with its low observed selectivity. This interpretation is further supported by the comparison of the free energy surfaces (FES) presented in Figures 2, 4, and 5, which indicates that the pathway toward glyoxylic acid is both kinetically less favorable and thermodynamically less preferred. Additionally, the trace amount of glyoxylic acid can undergo hydration in aqueous solution, facilitating its further oxidation to oxalic acid, which both transformation are low barriers (9.0, 4.2 kcal/mol) and thermodynamically favorable (-41.4, -7.0 kcal/mol). These results are depicted in Figures 7A and 7B as well as Figures 8A and 8B and explain trace formation of glyoxylic and oxalic acids as the secondary byproducts in the reaction network. Decomposition of glyoxylic and oxalic acids to small molecules such as $CO_2$, CO, $H_2O$ and HCOOH that is observed alongside the MD trajectories is shown in Figures 7A and 7B (C-C distances), which explains the carbon balance deficit in experiment.

**Additional control experiments: Product inhibition, effect of oxygen and catalyst(support)**

To investigate potential product inhibition glycolic acid was added to the glycolaldehyde solution. **Table 4**, entry **1** shows the standard reaction conditions, and entry 2 the effect of adding glycolic acid. The conversion significantly dropped (from 68 to 38%), while the selectivity and mass balance remained comparable, with a slight increase in glyoxylic acid (from 1 to 4%). Similar results were obtained earlier during the stability test of glycolic acid, in which 3% glyoxylic acid was formed (Table 2, entry 2). Based on these results, free glycolic acid appears to inhibit the conversion of glycolaldehyde. As it is discussed in the DFT section a $H^+$ transfer to the catalyst site can be probed alongside the simulation trajectory of glycolic acid formation that confirms catalyst inhibition due to the pH effect. Complete analysis of electronic charge and the interaction between various species in the reaction system and Pt catalyst we reported the complexation energies in **Figures S3-4** in SI.

View Article Online
DOI: 10.1039/D6CY00352D





**Table 4** Additional control experiments: 1wt% glycolaldehyde in 20 mL water, 100 mg 1w% Pt/C, 70 ˚C, 2 h, 10 bar oxygen pressure, stirring at 750 rpm.

| Entry | Variable | Conv. (mol%) | Glycolic acid sel. (mol%) | Glyoxylic acid sel. (mol%) | Oxalic acid sel. (mol%) | Carbon balance (mol%) |
|---|---|---|---|---|---|---|
| 1 | (Standard conditions) | 68 | 100 | 0.7 | 0 | 101 |
| 2 | Added 0.9 eq. GAc | 38 | 96 | 4.1 | 0 | 100 |
| 3 | 10 bar $N_2$ | 11 | 57 | 0 | 0 | 95 |
| 4 | 10 bar air | 68 | 98 | 0 | 0 | 99 |
| 5 | Activated Carbon | 19 | 15 | 0 | 7 | 89 |
| 6 | Blank | 20 | 11 | 12 | 7 | 84 |

A control experiment under nitrogen atmosphere ( Table 4, entry 3) shows an unexpected, yet low conversion of 11%, with a selectivity of only 57% to GAc. In contrast to the low selectivity to GAc, no consecutive products could be detected. These results indicate that under oxygen limitation conditions still some conversion of GAl can occur. The reaction under compressed air (Table 4, entry 4) shows similar results under standard conditions, i.e., 68% conversion and 98% selectivity to glycolic acid.

To investigate the influence of the catalyst support and the reaction medium itself on the oxidation of GAl, control experiments with only carbon support and a blank were also performed (Table 4, entries 5 and 6 respectively). Surprisingly, a considerable conversion of approximately 20% was observed in both cases, albeit with very low selectivity to GAc. The low carbon balance indicates the formation of either non-detected or gaseous products. Glycolaldehyde is a highly reactive molecule and in the presence of high pressure $O_2$ and high temperature undergoes various reactions such as decomposition and conversion to other small molecules if not converted into glycolic acid which is a more stable product. In the presence of active carbon, carbonyl group is polarized and surface reaction can also take place. Furthermore, as shown in **Scheme 1**, in aqueous solution several equilibria exist that produce other compound starting from glycolaldehyde.

A ca. 20% conversion which was observed in both blank and carbon-only control experiments, indicates the presence of parallel non-catalytic pathways. This background reactivity may arise from thermal decomposition and/or auto-oxidation due to high pressure $O_2$. These reactions can

View Article Online
DOI: 10.1039/D6CY00352D



also facilitate by activated carbon support. Hence, at elevated temperatures and high substrate concentrations the reactivity of glycolaldehyde can be enhanced.

**Catalyst stability**

To determine the stability of the Pt/C (1 wt%) catalyst, experiments on catalyst recyclability were performed. Data was collected from four consecutive experiments, performed under identical reaction conditions (1% substrate concentration, 70 °C, 10 bar oxygen, 2 h). For all experiments, the glycolaldehyde conversion and selectivity towards glycolic acid were determined. The results of the catalyst recycling studies are depicted in **Figure 9**. In the second run, a clear drop in the conversion of approximately 50% was observed. However, after this initial drop, runs three and four showed no significant further deactivation (within experimental error). To explain these results, catalyst characterization was performed on both the fresh catalyst, and the catalyst recovered after four runs. To determine if platinum leaching occurred, the metal loadings of both catalysts were compared. The Pt loading of the fresh catalyst (0.97-0.98 wt% Pt) was identical after 4 runs (0.96-0.97 wt% Pt). The concentration of Pt in the liquid phase was 0.5 ppm, corresponding to 0.01 mg of Pt, which is 1% of the initial Pt-intake.

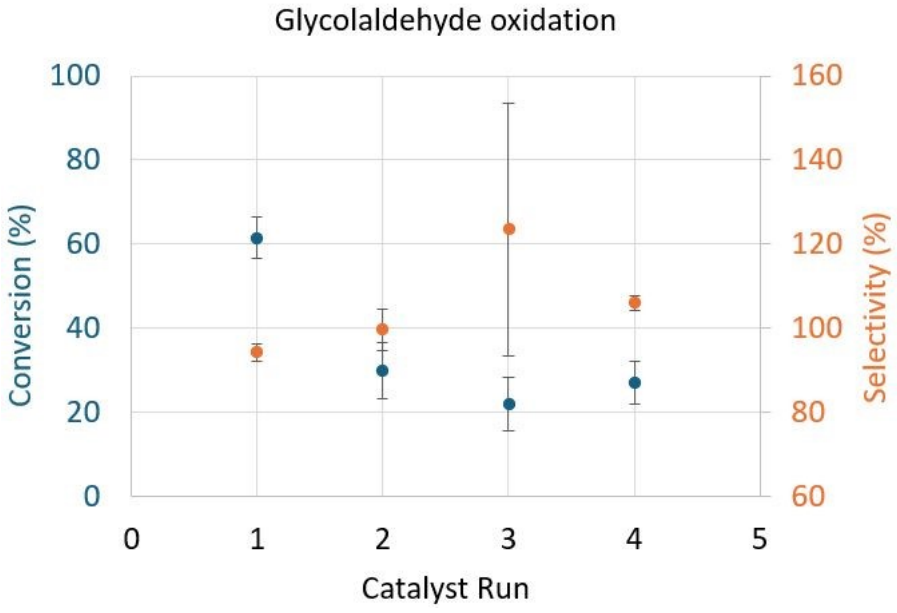


**Figure 9.** Results of the catalyst recycling study. Experimental conditions: 100 mg 1wt% Pt/C, 1wt% glycolaldehyde solution in 20 mL water, 70 ˚C, 2 h, 10 bar oxygen pressure, stirring at 750 rpm.

View Article Online
DOI: 10.1039/D6CY00352D



This indicates that metal leaching is not the reason for deactivation. TEM analyses of the fresh catalyst and the catalyst after 4 runs were compared and showed hardly any differences. The activated carbon support has a high surface area and micropores, which can trap substrate and product molecules near Pt sites. This results in high local concentrations near metal particles that may enhance re-adsorption of product and diffusion limitation inside the pores. Smaller platinum particles residing within the micropores may become inaccessible if those pores are obstructed.

The particle size of platinum nanoparticles were obtained by scanning transmission electron microscopy (STEM) coupled with high-angle annular dark-field imaging (HAADF). Representative STEM micrograph of fresh Pt/C catalyst is displayed in **Figure 10**. The average platinum nanoparticle size for the fresh catalyst was determined to be within the range of 0.5 to 2.5 nm. Furthermore, the Pt/C catalyst recovered after four catalytic cycle was subjected to STEM analysis. The mean platinum particle size of the recycled catalyst, even after the fourth operational cycle, remained within the 0.5-2.5 nm range (**Figure 11**). This observation indicates the robust stability of the platinum nanoparticles against sintering throughout the glycolaldehyde oxidation process under the specified *base free* reaction conditions.

X-ray photoelectron spectroscopy was utilized to ascertain the chemical composition and oxidation states of platinum on the catalyst surface. Analysis of the monometallic Pt/C catalyst's XPS spectrum revealed two distinct doublets within the Pt 4f core level, corresponding to Pt0, and Pt2+species. The predominant contribution originated from Pt0 (≈79%), with a minor presence of Pt2+(≈31%). Notably, no other higher oxidation states of platinum were detected (Figure 12A).

Additional XPS measurements were conducted to characterize the platinum species within the Pt/C catalyst following its utilization in glycolaldehyde oxidation, specifically examining both spent catalyst (after the 1st run) and samples after the 4th catalytic cycle. Prior to spectroscopic examination, the spent catalysts underwent thorough exhaustive washing with deionized water and subsequent drying in air at 378 K for a duration of 18 hours. The XPS spectrum of the spent catalyst (**Figure 12B**) revealed the persistent stability of Pt, thereby precluding deactivation mechanisms associated with the oxidation of platinum species under the applied reaction conditions.

Further confirmation of this stable platinum oxidation state was obtained from XPS analysis conducted on the Pt/C catalyst following its fourth consecutive cycle (**Figure 12C**). Collectively, the consistent oxidation states observed for platinum in the fresh, spent, and four-cycle recycled

View Article Online
DOI: 10.1039/D6CY00352D

catalysts strongly indicate the robustness of platinum's oxidation state throughout the glycolaldehyde oxidation process in *base-free* oxidation conditions.

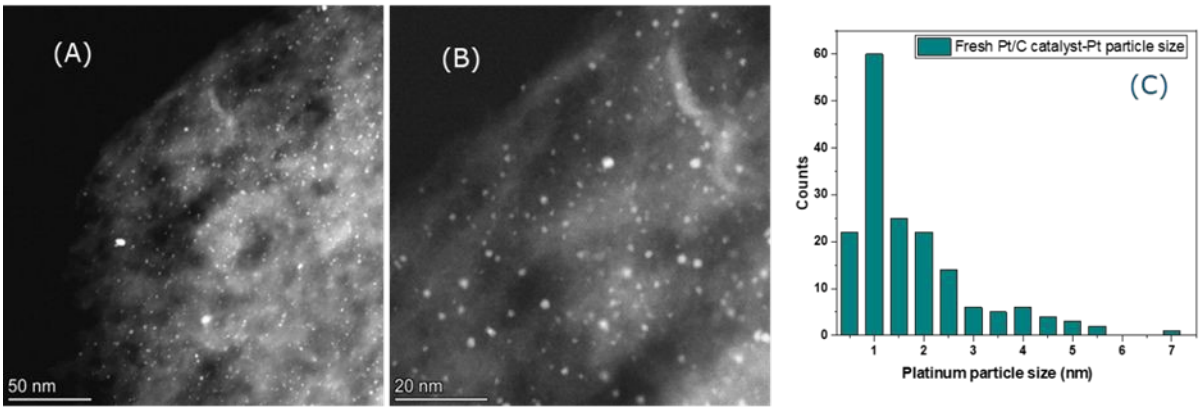


**Figure 10:** (A)&(B) STEM-HAADF image of fresh Pt/C catalyst under two magnifications (C) platinum particle size distribution.

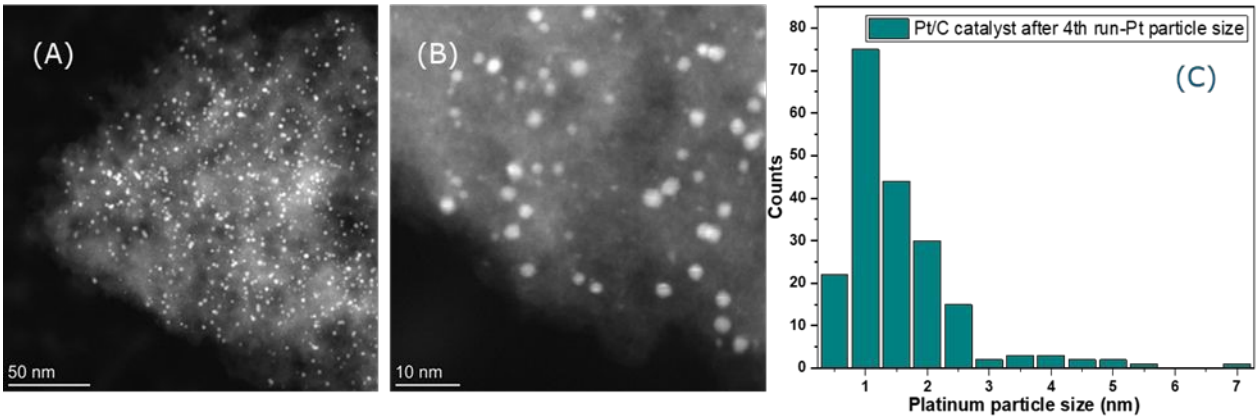


**Figure 11.** (A)&(B) STEM-HAADF image of recycled Pt/C catalyst after 4th run under two magnifications (C) platinum particle size distribution.

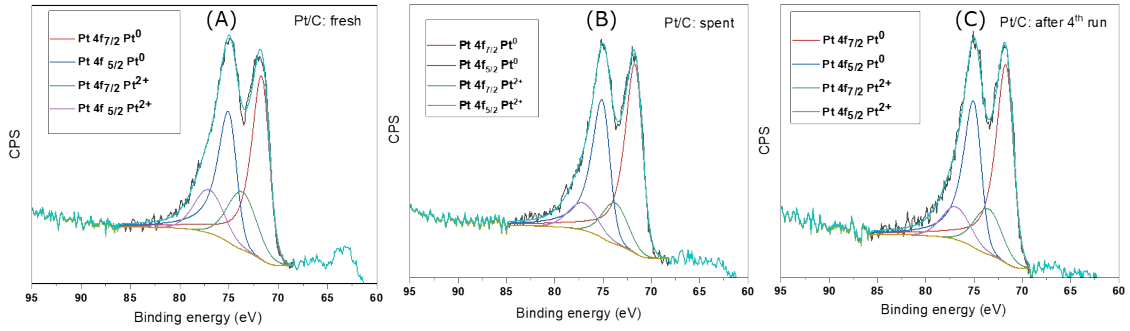

View Article Online
DOI: 10.1039/D6CY00352D

**Figure 12.** XPS spectrum of (A) fresh, (B) recycled (after 1st run) (C) recycled (after 4th run) Pt/C catalysts.

Next, the surface area of the carbon support was investigated with $N_2$-physisorption. The results are reported in **Table 5.**

**Table 5.** $N_2$ physisorption of 1wt% Pt/C (fresh and after 4 runs)

| Entry | 1wt% Pt/C Catalyst | **Surface area ($m^2/g$)[a]** | **Pore volume ($cm^3/g$)[b]** | **Average pore size (Å)[c]** |
|---|---|---|---|---|
| 1 | Fresh | 581 | 320 | 62 |
| 2 | After 4 runs | 471 | 249 | 60 |

*[a]Calculated from $N_2$ physisorption using the BET equation. [b]Calculated from $N_2$ physisorption using the t-plot method. [c]Calculated from $N_2$ physisorption using the BJH formula using 4V/A from BET.*

In line with the catalyst stability tests the complete analysis of the possible interactions between $Pt_4$ catalyst and the reactant, main product and possible consecutive side products as well as $Pt_4$ and carbon support are analyzed in **SI Figures S3, S4** and **Table S3.** Based on this analysis strong interactions between carbonyl and OH groups of the various species and Pt atoms can be detected. The strongest interaction can be observed between glyoxylic acid carbonyl and $Pt_4$.

As discussed in previous part, after production of the main and side products the Pt atoms can be covered (reduced) with $H^+/H^-$ ions, which requires to be oxidized to Pt(0) to maintain its catalytic activity. In **Figure 13A** the energetics of regeneration of the hydrated Pt atoms reaction using $O_2$ is depicted (a barrier of 9.0 kcal/mol and reaction free energy of -3.0 kcal/mol are calculated).

Generated $H_2O_2$ in the reaction medium may further react with glycolaldehyde hydrate and glycolic acid to produce glycolaldehyde peroxide and peroxy acid species. We have calculated the energetics of both compounds without involvement of Pt/C catalyst and only in presence of water and $H_2O_2$. These two transformations are rather high barrier reactions with 50.0 and 68.0 kcal/mol for glycolaldehyde hydrate and glycolic acid, respectively. However, according to the calculations, the peroxide and peroxy acid are not stable and very quickly decompose to $CH_2O$, HCOOH and $CO_2$ after formation. A similar experimental observation has been reported in literature.[54]

As a competitive possible reaction related to the $H_2O_2$ formation ($O_2$ and $Pt\cdots H^+/Pt\cdots H^-$) we simulated the $H^+/H^-$ transfer to glycolaldehyde instead of $O_2$, which can be present in the reaction environment and results in formation of ethylene glycol. The mechanism and FES are depicted in **Figure 13B.** Similar to $H_2O_2$ formation this reaction has a low barrier and (8.5 kcal/mol) and is

View Article Online
DOI: 10.1039/D6CY00352D

strongly exergonic. However, in our experiments there is no evidence of formation of ethylene glycol which can be attributed to the fast full conversion of glycolaldehyde and more availability of $O_2$ in the proximity of $PtH_2$. Furthermore, in aqueous solution the majority of glycolaldehyde is the hydrate form which is not $H^+/H^-$ acceptor.

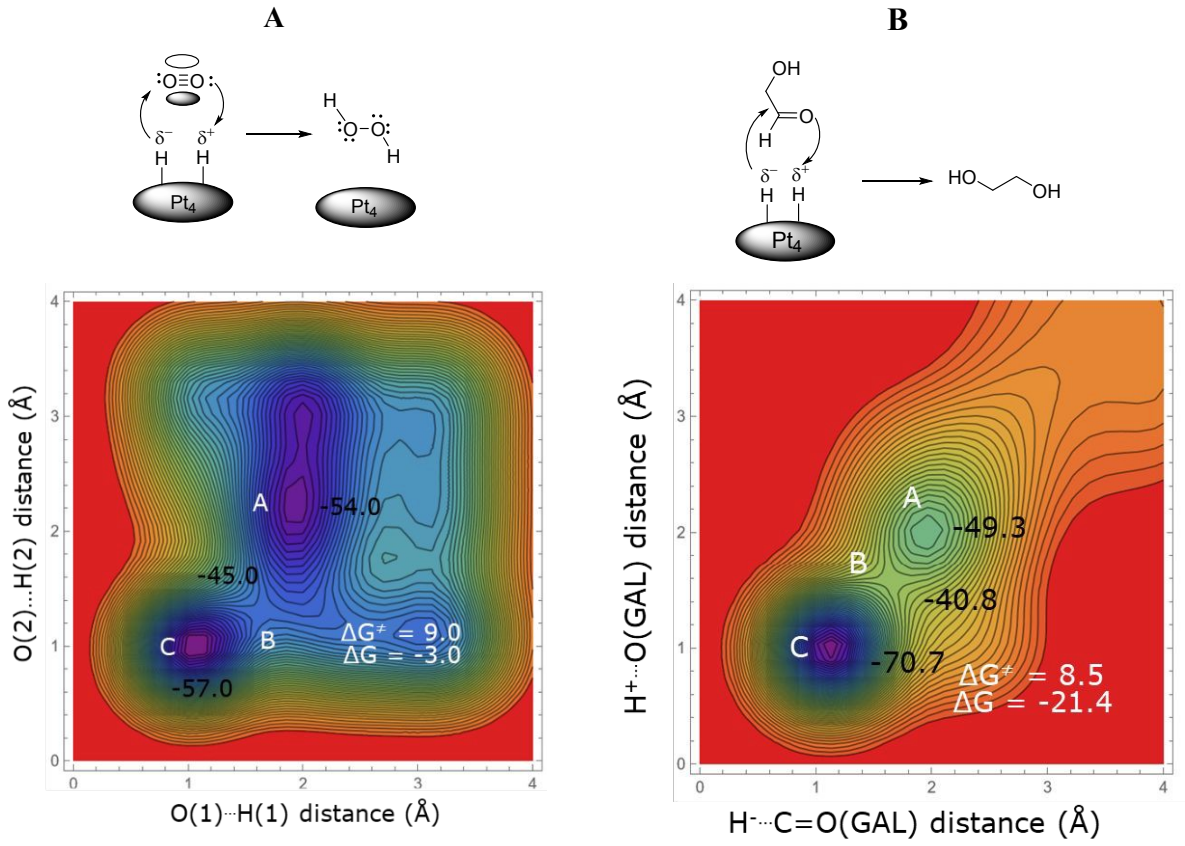


**Figure 13. A)** The available oxygen in the reaction atmosphere abstracts $H^+/H^-$ from the catalyst and reactivates the Pt atoms. **B)** Alternatively, $H^+/H^-$ on the Pt atoms can interact with glycolaldehyde to produce ethylene glycol.

**Scheme 2** summarizes the desired reaction which is conversion of glycolaldehyde dimer to glycolic acid (singled out with green). Consecutive side products such as glyoxylic acid and its hydrate form, oxalic acid, formic acid, ethylene glycol and $CO_2$ can be produced alongside the main reaction through further oxidation of glycolic acid (singled out with red), however, with remarkably high barriers than the main pathway. This is in agreement with our experimental observations that the side products are not detected in the reaction environment.

View Article Online
DOI: 10.1039/D6CY00352D



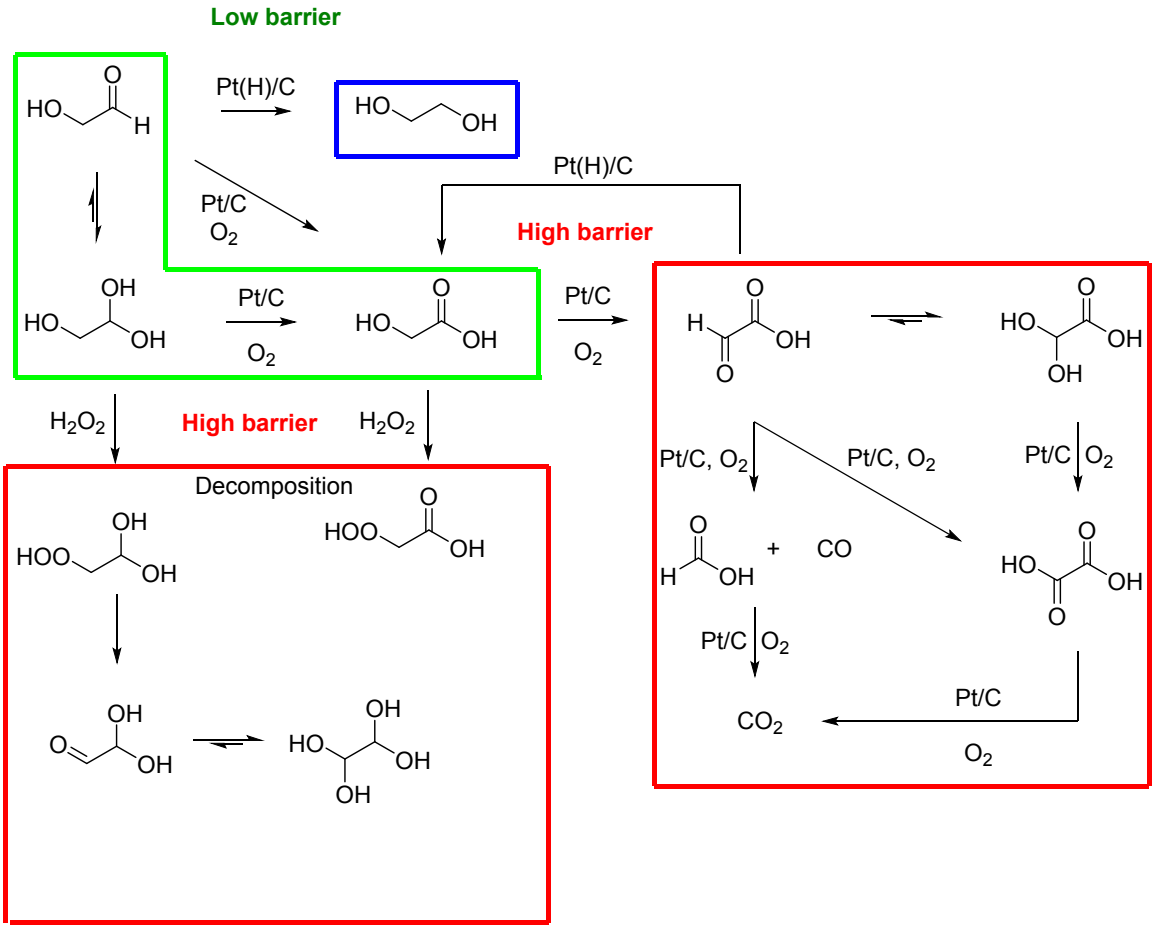


**Scheme 2.** Suggested reaction network: intended (green) versus undesired (blue, red) pathways.

## Summary and conclusions

In this work we investigated the catalytic oxidation of glycolaldehyde to glycolic acid using a platinum on activated carbon catalyst (Pt/C). The optimal reaction conditions were obtained by a Design of Experiment and statistical analysis and verified by experiments. The experimental results showed high selectivity, conversion and carbon balance toward glycolic acid at 70 ˚C, 7 hours and 10 bar oxygen. The stability of the main product glycolic acid and feasible consecutive side products such as glyoxylic acid, oxalic acid, formic acid, glyoxal and formaldehyde was investigated, showing that glycolic acid is quite stable , while the rest were completely converted to the volatiles such as $CO_2$. Additional control experiments performed under various conditions showed that the conversion of GAl dramatically decreases in absence of oxygen or catalyst. Furthermore, the presence of GAc from the start of the reaction also suggested product inhibition, or possibly a strong pH effect. The effects of substrate and catalyst concentration were investigated

View Article Online
DOI: 10.1039/D6CY00352D

and it was found that as expected, increasing glycolaldehyde concentration results in a lower conversion to glycolic acid. More unexpected was the decrease in glycolaldehyde selectivity and carbon balance with increasing Pt to substrate ratio. Catalyst stability tests and characterisations (HAADF-STEM, BET, XRD, XPS, Elemental analysis) confirm that Pt/C is a promising catalyst for the selective oxidation of GAl to GAc. Using DFT metadynamics simulations in a periodic system at 343K, FESs were calculated at heterogeneous phase to gain more insights about the reaction mechanisms and help explain the experimental observations. DFT results showed that the hydrate form of glycolaldehyde is the dominant structure in a diluted reaction medium. The glycolaldehyde hydrate conversion to glycolic acid has a lower activation barrier than the glycolaldehyde monomer which is in line with the higher observed conversion rate in a diluted reaction mixture.

A rather high barrier and unfavorable thermodynamics for the subsequent glycolic to glyoxylic acid conversion support the stability of the main product. On the other hand, favorable thermodynamics and kinetics of glyoxylic and oxalic acid decomposition confirms their low stability at 343 K, and hence full conversion during control reactions. The results of this work pave the way in utilizing bio-based resources and agricultural residues to obtain bio-glycolic acid for further application in bio-renewable materials.

## Acknowledgements

This work used the Dutch national e-infrastructure with the support of the SURF Cooperative using grant no. EINF-9485. This research was financed by TKI funding from the Topconsortia for Knowledge & Innovation (TKI's) of the Ministry of Agriculture, Fisheries, Food Security and Nature (LVVN, project LWV22223, Production of glycolic acid from renewable resources (bio-GA)) and the companies Archer Daniels Midland Company for providing catalysts and bio-based feedstock, Will & Co., and WeylChem for providing various types of Pt4/C catalysts and constructive feedback. We thank Mr. Jelmer Vrom for TEM measurements and Ms. Nadine Dieterman for physisorption measurements.

## Supporting Information

Design of Experiment data, HPLC chromatograms related to the Tables 1, 3, 4 in the main text, analytical details related to the HPLC measurements, calculation of kinetics and thermodynamics of various glycolaldehyde species in aqueous and acidic solution, complexation energies between Pt and all species in the reaction environment, xyz coordinates of the reactant, transition state and product structures obtained by (TRACE_IRC code) shown in the FESs in the main text.

## References

View Article Online
DOI: 10.1039/D6CY00352D



1. D. Mohan; C. U. Pittman, P. H. Steele, Energy & Fuels 2006, 20 (3), 848-889 DOI: 10.1021/ef0502397.
2. P. Kostetskyy , M. W. Coile , J. M. Terrian , J. W. Collins, K. J. Martin, J. F. Brazdil , L. J. Broadbelt, Journal of Analytical and Applied Pyrolysis, 2020, 149, 104846.
3. A. Gonzalez-Quiroga, K. M. Van Geem, G. B. Marin, Biomass Conv. Bioref. (2017) 7:305–317.
4. C. Bækhøj Schandel, M. Høj, C. M. Osmundsen, M. J. Beier, E. Taarning, A. D. Jensen, ACS Sustainable Chem. Eng. 2021, 9, 1, 305–311 https://doi.org/10.1021/acssuschemeng.0c07232
5. K. C. Mathews, Biochemistry. K. E. Van Holde, 2000, Ahern, Kevin G. (3rd ed.). San Francisco, Calif. Benjamin Cummings. p. 280. ISBN 978-0-8053-3066-3. OCLC 42290721.
6. N. F. Kleimeier, A. K. Eckhardt, R. I. Kaiser, J. Am. Chem. Soc. 2021, 143 (34): 14009–14018, doi:10.1021/jacs.1c07978.
7. H. Chi, Z. Liang, S. Kuang, Y. Jin, M. Li, T. Yan, J. Lin, S. Wang, S. Zhang, X. Ma, Nat Commun. 2025, 16(1):979. doi: 10.1038/s41467-025-56104-5.
8. C.-A. Chen, Y. W. Chen. US 9.126,912 B1, Processes for preparing formaldehyde, glycolaldehyde and ethylene glycol.
9. C. M. Osmundsen, E. Taarning, WO2018095973A1, A method and a system for producing glycolic acid and/or glycolate (Pt on activated carbon)
10. Z. Yan, B. Kusema, S. Streiff, WO/2020/258131, METHOD FOR PREPARING GLYCOLIC ACID.
11. Yu Han, Jizhe Zhang, X. Liu, Molybdenum-containing Acidic Catalysts to Convert Cellulosic Biomass to Glycolic Acid. US20130281733A1, 2013.
12. C. K. Acharya, D. I. Sullivan, C. Heath Turner. J. Phys. Chem. C 2008, 112, 13607–13622
13. Y. Liu, J. Dai, N. Liu, Y. Wu, J. Huang, Y. Zheng, Q. Li, ACS Sustainable Chem. Eng. 2021, 9, 7255−7266.
14. V. Perazzolo, R. Brandiele, C. Durante, M. Zerbetto, V. Causin, G. A. Rizzi, I. Cerri, G. Granozzi, A. Gennaro. ACS Catal. 2018, 8, 1122−1137.
15. S. Wu, Y. Quan, J. Ren, Front. Chem. Sci. Eng. 2025, 19(8): 72, https://doi.org/10.1007/s11705-025-2585-7
16. X. Liu, M. Zou, Y. Yu, Y. Hai, J. Huang, Y. Fan, Y. Zhang, Y. Weng, Y. Liao, Ind. Eng. Chem. Res. 2025, 64, 10453−10461.
17. R. K. Pazhavelikkakath Purushothaman, F. van der Klis, A. E. Frissen, J. van Haveren, A. Mayoral, A. van der Bent, D. S. van Es, Green Chem., 2018,20, 2763-2774.
18. F. van der Klis, L. Gootjes, J. van Haveren, D. S. van Es, J. H. Bitter. React. Chem. Eng., 2018, 3, 540–549.
19. F. van der Klis, L. Gootjes, N. H. Verstijnen, J. van Haveren, D. S. van Es, J. H. Bitter, RSC Adv., 2022, 12, 8918–8923
20. R. K. Pazhavelikkakath Purushothaman, J. van Haveren, I. M. Cabrera, E. R. H. van Eck, H. J. Heeres, ChemSusChem 2014, 7, 1140 – 1147.
21. F. van der Klis, L. Gootjes, J. van Haveren, D. S. van Es, J. H. Bitter, Green Chem., 2015, 17, 3900 – 3909.
22. a) H. Q. Fu, B. F. Su, H. Q. Yang, C. W. Hub, RSC Adv., 2015, 5, 40978; b) J. Pan, E. Strugovshchikov, A. Salóm-Catala, G. Novell-Leruth, K. Kaźmierczak, D. Curulla-Ferré, J. J. Carbó, C. Godard, J. M. Ricart, J. Phys. Chem. C 2025, 129, 2477−2487.

View Article Online
DOI: 10.1039/D6CY00352D



23. A. C. Garcia, M. J. Kolb, C. van Nierop y Sanchez, J. Vos, Y. Y. Birdja, Y. Kwon, G. Tremiliosi-Filho, M. T.M. Koper, ACS Catal. 2016, 6, 7, 4491–4500, https://doi.org/10.1021/acscatal.6b00709.
24. G. Yan, Z. Gao, M. Zhao, K. Ma, Z. Ding, W. Yang, X. Ding, Molecular Catalysis 497 (2020) 111205.
25. Z. Hui-Wen, L. Chun-Hai, R. Yu-Rong, L. Yi, Z. Yong-Fan, C. Wen-Kai,. Acta Phys. -Chim. Sin. 2016, 32, 1183 – 1190. doi: 10.3866/PKU.WHXB201603032
26. Y. Wang, J. Ding, F. Deng, H. Liu, Carbon Letters (2024) 34:1593–1608.
27. a) C. Cui, Z. Luo, J. Yao, CCS Chem. 2019, 1, 215–225. b) R. Sechi, T. Höltzl J. Phys. Chem. A 2023, 127, 21, 4596–4608. c) E. Fernández, L. Liu, M. Boronat, R. Arenal, P. Concepcion, A. Corma, ACS Catal. 2019, 9, 11530−11541, 10.1021/acscatal.9b03207. d) B. Hammer, J. K. Nørskov, Nature 1995, 376, 238–240. e) T. J. Dhilip Kumar, C. Zhou, H. Cheng, R. C. Forrey, N. J. Balakrishnan, J. Chem. Phys. 2008, 128, 124704.
28. Hongqing Shi, Amanda S. Barnard, Ian K. Snook. Quantum mechanical properties of graphene nano-flakes and quantum dots. Nanoscale, 2012, 4, 6761–6767
29. H. Shi, A. S. Barnard, I. K. Snook, J. Mater. Chem., 2012, 22, 18119–18123.
30. A. S Barnard, I. K Snook. Modelling Simul. Mater. Sci. Eng. 19 (2011) 054001
31. P. J. F. Harris1, Z. Liu, K. Suenaga, J. Phys.: Condens. Matter 20 (2008) 362201.
32. A. Vargas, T. Bürgi, A. Baiker. Journal of Catalysis 222 (2004) 439–449.
33. L. Partanen, K. Laasonen. Phys. Chem. Chem. Phys., 2024, 26, 18233.
34. a) J. Vande Vondele, M. KracK., F. Mohamed, M. Parrinello, T. Chassing, J. Hutter, Comput. Phys. Commun. 2005, 167, 103-128. b) T. D. Kühne, et al., J. Chem. Phys. 2020, 152, 194103.
35. S. Goedecker , M. Teter, J. Hutter, Phys. Rev. B, 1996, 54, 1703. c) M. K. Sabbe, M.-F. Reyniersa, K. Reuter, Catal. Sci. Technol., 2012, 2, 2010–2024, doi.org/10.1039/C2CY20261A
36. P. J. Perdew, K. Burke, M. Ernzerhof, Physical Review letters (1996), 77 (18), 3865-3868
37. S. Grimme, J. Antony, S. Ehrlich, H. Krieg, J. Chem. Phys. 2010, 132, No. 154104.
38. A. Laio, M. Parrinello, Proc. Natl. Acad. Sci. U.S.A. 2002, 99, 12562.
39. M. Invernizzi, M. Parrinello, J. Phys. Chem. Lett. 2020, 11, 2731.
40. M. Bonomi M., D. Branduardi, G. Bussi, C. Camilloni, D. Provasi, P. Raiteri, D. Donadio, F. Marinelli, F. Pietrucci, R. A. Broglia, et al. Comput. Phys. Commun. 2009, 180, 1962.
41. a) M. Heshmat, M. Leven, O. Linker, M. Sebastian, C. Gürtler, M. R. Machat, Phys. Chem. Chem. Phys., 2023,25, 20485-20494, DOI: 10.1039/D3CP03146B., b) D. Brüggemann, M. R. Machat, R. Schomäcker, M. Heshmat, Polymers 2024, 16(1), 136; https://doi.org/10.3390/polym16010136, c) M. Heshmat, J. Phys. Chem. C 2020, 124, 20, 10951–10960, https://doi.org/10.1021/acs.jpcc.0c01088.
42. R. Ketkaew, F. Creazzo, K. Sivula, S. Luber, Chem Catalysis 4, 101085, September 19, 2024, DOI:10.1016/j.checat.2024.101085
43. F. Creazzo, K. Sivula, S. Luber, iScience 28, 112045, March 21, 2025, DOI:10.1016/j.isci.2025.112045
44. R. Verduci, et al., J. Am. Chem. Soc. 2024, 146, 26, 18061–18073, DOI:10.1021/jacs.4c05042
45. a) L. Liu, B. Lukose and B. Ensing, ACS Catal, 2018, 8, 3376. b) B. Ensing, A. Laio, M. Parrinello and M. L. A. Klein, J. Phys. Chem. B, 2005, 109, 667645, DOI: 10.1021/jp045571i
46. a) B. Ensing, M. L. Klein, Proc. Natl. Acad. Sci., USA 2005, 102, 6755-6759 DOI: 10.1073/pnas.0408094102. b) B. Ensing, M. De Vivo, Z. Liu, P. Moore, M. L. Klein, Acc. Chem. Res. 2006, 39, 73-81 DOI: 10.1021/ar040198i
47. W. Humphrey, A. Dalke, K. Schulten, J. Molec. Graphics, 1996, 14, 33.

View Article Online
DOI: 10.1039/D6CY00352D

48. http://www.ks.uiuc.edu/Research/vmd/
49. J. Kua, M. M. Galloway, K. D. Millage, J. E. Avila, D. O. De Haan, J. Phys. Chem. A 2013, 117, 2997−3008, dx.doi.org/10.1021/jp312202j
50. G. C. S. Collins, W. O. George, (1971). Journal of the Chemical Society B: Physical Organic: 1352. doi:10.1039/j29710001352. ISSN 0045-6470
51. Y. A. Varoujan, S. Harty-Majors, A. A. Ismail, (1998). Carbohydrate Research. 309: 31–38. doi:10.1016/S0008-6215(98)00129-3
52. R. V. Lenth, Journal of Statistical Software, 2009, 32, , 1 – 17. https://doi.org/10.18637/jss.v032.i07
53. M. Ai, K. Ohdan, Bulletin of the Chemical Society of Japan, 70, 1997, 1995–1999, https://doi.org/10.1246/bcsj.70.1995.
54. L. Liu, X. Zhang, Z. Li, Y. Zhang, M. Ge, Chemosphere 186 (2017) 430e437
55. H. S. Fry, K. L. Milstead, J. Am. Chem. Soc. 1935, 57, 11, 2269–2272, https://doi.org/10.1021/ja01314a068.



View Article Online
DOI: 10.1039/D6CY00352D

**Dear Dr. Maria Southall,**

The authors declare that the data supporting this article have been included as part of the Supplementary Information.

Best regards,

Dr. Mojgan Heshmat

Wageningen Food & Biobased Research

Bornse Weilanden 9, 6708 WG Wageningen, The Netherlands

Wageningen Campus | Building 118 (Axis), Phone: +31 (0) 317481375